Arabian Journal of Chemistry (2023) **16**, 104911

King Saud University

Arabian Journal of Chemistry

www.ksu.edu.sa
www.sciencedirect.com

ORIGINAL ARTICLE

Vasodilatory constituents of essential oil from *Nardostachys jatamansi* DC.: Virtual screening, experimental validation and the potential molecular mechanisms

Bian-Xia Xue [a,1], Si-Xia Liu [a,1], Patrick Kwabena Oduro [a], Nana Ama Mireku-Gyimah [b], Li-Hua Zhang [a,*], Qilong Wang [a,*], Hong-Hua Wu [a,*]

[a] *State Key Laboratory of Component-based Chinese Medicine, Institute of Traditional Chinese Medicine, Tianjin University of Traditional Chinese Medicine, 10 Poyanghu Road, West Area, Tuanbo New Town, Jinghai District, Tianjin 301617, People's Republic of China*
[b] *Department of Pharmacognosy and Herbal Medicine, School of Pharmacy, College of Health Sciences, University of Ghana, Legon-Accra, Ghana*

Received 18 December 2022; accepted 9 April 2023
Available online 17 April 2023

KEYWORDS

Nardostachys jatamansi DC;
Essential oil;
GC/MS;
Vasodilatation;
Spectrum-effect relationship;
Network pharmacology

Abstract Recent studies have demonstrated that the essential oil of *Nardostachys jatamansi* (EONJ) has potential health benefits, such as reducing blood pressure, protecting the heart, and relaxing blood vessels. However, the active constituents and the underlying molecular mechanisms are still unclear. In this study, we utilized GC–MS to identify the chemical constituents of EONJ and tested its vasodilatory effects on constricted isolated thoracic aorta rings from mice. We then combined network pharmacology with spectrum-effect relationship approaches to select potential marker ingredients and uncover the possible vascular protective mechanism of EONJ. Among the four main chemicals screened in this work, β-maaliene and patchouli alcohol exhibited varying levels of vasodilatory effects on isolated, constricted thoracic aortic rings. Bioinformatics and network pharmacology analyses revealed that EONJ's primary biological regulation targets were NOS3 and PTGS2. Moreover, EONJ may exert its vasodilatory effects by modulating lipid and

* Corresponding authors at: Institute of Traditional Chinese Medicine, Tianjin University of Traditional Chinese Medicine, 10 Poyanghu Road, West Area, Tuanbo New Town, Jinghai District, Tianjin, 301617, China.
E-mail addresses: zhanglihua200061@163.com (L.-H. Zhang), wangqilong_00@tjutcm.edu.cn (Q. Wang), wuhonghua2011@tjutcm.edu.cn (H.-H. Wu).
[1] Co-first authors: B.-X. Xue and S.-X. Liu contributed equally to this work and should be considered co-first authors.
Peer review under responsibility of King Saud University.

Production and hosting by Elsevier

https://doi.org/10.1016/j.arabjc.2023.104911

atherosclerosis and the PI3K-AKT signaling pathways. This study provides the first report on the vasodilatory effects and possible molecular mechanisms of EONJ. The findings may serve as a reference for quality evaluation, identification of bioactive markers, and future applications of EONJ in the prevention and treatment of vascular and cardiac diseases.

1. Introduction

Nardostachys jatamansi DC., belonging to the Caprifoliaceae family of perennial herbs, is an endangered medicinal and aromatic plant distributed predominantly at the high elevation of 3300–5000 m in China, Nepal, India, Bhutan, and other countries (Chauhan et al., 2011; Rehman and Ahmad, 2019). *N. jatamansi* has been used as a medicine for a long time, and it is often given to people with diseases of the nervous, digestive, cardiovascular systems, and skin. Notably, *N. jatamansi* has great therapeutic potential in the treatment of cardiovascular diseases, especially hypertension (Bhat and Malik, 2020; Lyle et al., 2009). Recently, a clinical trial was conducted to show that *N. jatamansi* can significantly decrease systolic and diastolic blood pressure in patients with essential hypertension (Bhat and Malik, 2020). The aqueous extract of *N. chinensis* Batalin exhibited hypotensive and protective effects in hypertensive rats with two-kidney one-clip (2K1C)-induced myocardial hypertrophy (Aisa et al., 2017). The methanol extract of *N. jatamansi* can inhibit angiotensin-converting enzymes leading to a probable decrease in blood pressure (Bose et al., 2019). More importantly, our previous study demonstrated a significant vasodilatory effect of the total methanolic extract and the ethyl acetate fraction of *N. jatamansi* (Fang et al. (2022). The two low polar constituents, (-)-aristolone and kanshone H, are the major compounds with significant vasodilation properties. Owing to this, we are curious to know whether the essential oil of *N. jatamansi* (EONJ) has similar vasodilatory activity.

To the best of our knowledge, the EONJ is one of the most important components of *N. jatamansi,* with various industrial applications such as shampoo, soap, bath foam, perfume, incense in religious ceremonies, and so on. It is also noted as one of the key quality control markers of *N. jatamansi* in the Chinese Pharmacopoeia, which stipulates that the EONJ content should not be less than2.0% (mL/g) (China Pharmacopoeia Committee, 2020b). To date, gas chromatography-mass spectrometry (GC–MS) has been frequently employed for the qualitative and semi-quantitative profiling of EONJ. It has been investigated in depth by a considerable number of scholars (Chauhan et al., 2017; Gen et al., 2011; Han et al., 2017; Jin et al., 2018a; Jin et al., 2018b; Maiwulanjiang et al., 2015; Takemoto et al., 2008; Tanaka and Komatsu, 2008; Wang et al., 2015; Wu et al., 2015). The major constituents of EONJ vary depending on species and origins. They might also change along with the drying degree as well as the processing temperature of the herb (Chauhan et al., 2017; Wang et al., 2021). Moreover, it has been extensively investigated for various pharmacological activities. It is notable for its promising efficacy in terms of cardiovascular disease, such as the treatment of cardiomyocyte death, salt-sensitive hypertension, arrhythmias, and myocardial ischemia–reperfusion injury (Cao et al., 2010; Jiang et al., 2017; Maiwulanjiang et al., 2014; Yang et al., 2010; Yang et al., 2018). Maiwulanjiang et al. have discovered that the EONJ is the main ingredient that could trigger vasodilation. However, the specific active constituents remain unknown (Maiwulanjiang et al., 2015).

Recently, screening bioactive candidates from herbal medicines has become a serious challenge owing to their intrinsic properties of diverse components, multi-targets, integrative regulation, and complex mechanisms (Zhang et al., 2018). Traditionally, the screening of bioactive ingredients in herbal medicines has been carried out by conventional methods, *viz*. extraction, purification, structural identification of phytoconstituents and finally bioassays, which are time-consuming and inefficient. Nowadays, numerous researchers have exploited fingerprint-activity relationship models to uncover promising bioactive constituents, including hierarchical cluster analysis (HCA) (Liu et al., 2021), principal component analysis (PCA) (Cai et al., 2019; Liu et al., 2021), gray correlation analysis (GCA) (Chen et al., 2019; Xiao et al., 2018; Yuan et al., 2022; Zhang et al., 2019a), partial least squares regression analysis (PLSR) (Guo et al., 2020; Shawky et al., 2018; Zhang et al., 2019b), bivariate correlation analysis (BCA) (Yuan et al., 2022; Pang et al., 2022), multiple linear regression analysis (MLRA) (Cai et al., 2019; Kong et al., 2017; Zhang et al., 2018), and back propagation-artificial neural network modeling (BP-ANN) (Guo et al., 2020; Wang et al., 2017). Furthermore, the network pharmacological approach has often been integrated into the systematic virtual screening of the core targets and the primary bioactive ingredients from herbal medicines (Cheng et al., 2021; He et al., 2019; Jia et al., 2021; Zeng et al., 2022).

Hence, the GC–MS technique was applied to analyze the chemical compositions of four EONJs, whose significant vasodilatory effects were reported herein. Furthermore, a combination of the spectrum-effect relationship and network pharmacology was integrated for mining the vasodilatory constituents of EONJ and their potential targets, as well as the possible molecular mechanisms.

2. Materials and methods

2.1. Plant material and reagents

The roots and rhizomes of *Nardostachys jatamansi* DC. were purchased from Beijing Tong Ren Tang Tianjin Nankai Pharmacy Co. Ltd. (batch number: 20211220; origin: Sichuan province, China) and were authenticated by Prof. Tianxiang Li of Tianjin University of Traditional Chinese Medicine, China. Voucher specimens were deposited in the State Key Laboratory of Component Chinese Medicines, Institute of Chinese Medicine, Tianjin University of Traditional Chinese Medicine. NJ-B, the essential oil of sample B of *N. jatamansi*, sourced from Sichuan, was kindly supplied and produced by one of our partners in a Wenxin Keli-related project, Shandong BUCHANG Pharmaceutical Co. Ltd. NJ-C, the essential oil of sample C of *N. jatamansi* (batch number: 8208), namely 'Spikenard C', was originated in Nepal and made in the UK by Shirley Price Aromatherapy Ltd., 8 Hawley Road, Hinckley Leicestershire UK LE10 OPR. NJ-D, the essential oil of sample D of *N. jatamansi* (batch number: 210259A), namely 'Spikenard D', was purchased from dōTERRA Intl, LLC, 389 South 1300 West Pleasant Grove, UTAH 84062, U.S.A., and the place of origin was unknown. C_8–C_{40} alkanes calibration standard (SIGMA-ALDRICH, 40147-U, USA) was employed as the retention index standard in this work, consisting of a mixture of aliphatic hydrocarbons dissolved in *n*-hexane. Sodium chloride (NaCl), sodium bicarbonate ($NaHCO_3$), and D-glucose were purchased from Damao

Chemical Reagent Factory (Tianjin, China). Magnesium sulfate heptahydrate ($MgSO_4{\cdot}7H_2O$) was obtained from Tianjin Guangfu Technology Development Co. (Tianjin, China). Potassium chloride (KCl) was available from Boote (Tianjin) Chemical Trading Co. (Tianjin, China). Potassium dihydrogen phosphate anhydrous (KH_2PO_4), Crystalline calcium chloride ($CaCl_2{\cdot}2H_2O$) were acquired from Tianjin Bailens Biotechnology Co. (Tianjin, China). Dimethyl sulfoxide (DMSO), U46619(9,11-methanoepoxy PGH2), acetylcholine (Ach), and sodium nitroprusside (SNP) used in the experiment were purchased from Sigma-Aldrich (St. Louis, MO). Isoflurane was sourced from Rayward Life Technology Co., Ltd (Shenzhen, China). Patchouli alcohol was purchased from Sichuan Victory Biological Technology Co., Ltd (China) with a purity determined by GC analysis as above 98%.

2.2. Extraction and sample preparation

The essential oil was extracted from 30 g powder of dried *N. jatamansi* (sieved through 50 mesh) by hydro-distillation for 4 h in 600 mL of distilled water, using Clevenger-type apparatus and following the standard procedure described in the Chinese Pharmacopoeia (2020 Edition, Part IV) (China Pharmacopoeia Committee, 2020a), until there was no significant increase of the volume of oil collected. The volume of volatile oil was measured and recorded by the graduated tube and the yield was calculated. The yields were expressed as the volume of oil/weight of plant material (% *v*/*w*). The essential oil collected was dried over anhydrous sodium sulfate, dissolved in ethyl acetate (1:500, *v*/*v*), filtered through a 0.22 μm microporous membrane, and stored in an amber-colored sealed vial at a 4 °C in a refrigerator for further analysis. Thus, the essential oil sample A of *N. jatamansi* (NJ-A) was obtained. Similarly, NJ-B, NJ-C and NJ-D were dissolved in ethyl acetate (1:500, *v*/*v*), filtered through a 0.22 μm microporous membrane, and kept in an amber-colored sealed vial at 4 °C for the subsequent experiments.

2.3. Isolation and identification of the main constituents

NJ-B (2 mL, 1.83 g) was dissolved in methanol-tetrahydrofuran (1:1) and filtered by 0.45 μm microporous filter before isolation of the main constituents by preparative HPLC. NJ-B was separated on a Gilson GX-281 preparative-HPLC system equipped with a Luna C18(2) column (250 × 21.2 mm, 5 μm) at room temperature. The mobile phase was composed of H_2O (A) and acetonitrile (B) and implemented in the gradient elution as follows: 80 ∼ 100% A for 12 min; 100% A was kept for 15 min. The flow rate was set as 15 mL/min, and the detection wavelength was selected at 220 and 254 nm. The purity of the isolated phytochemicals was determined by GC–MS and LC-MS. Their structures were identified by analysis of the GC–MS, ^{1}H, and ^{13}C NMR data, as well as the comparison of their NMR data with those reported. Three main constituents were then afforded and identified as valerena-4,7(11)-diene (3.28%, 60.0 mg, t_R = 2.25 min, purity of 99.14%) (Paul et al., 2001), calarene (18.03%, 330 mg, t_R = 2.57 min, purity of 99.21%) (Abraham et al., 1992; Nagashima et al., 1997;Furusawa et al., 2006) and β-maaliene (3.39%, 62.0 mg, t_R = 2.89 min, purity of 96.00%) (Abraham et al., 1992).

Valerena-4,7(11)-diene: Colorless oil; [α]20 D −0.32 (*c* 0.125, ACN); UV (ACN) λ_{max} 214 nm; CD (*c* 1.00, ACN) λ (Δε) 204 (-0.43) nm, 228 (1.02) nm; ^{1}H NMR (400 MHz, $CDCl_3$) δ_H (mult, *J* in Hz): 0.76 (3H, d, 7.2), 1.28–1.36 (2H, m), 1.49–1.57 (2H, m), 1.64 (3H, s), 1.66 (3H, s), 1.69 (3H, s), 1.79–1.85 (2H, m), 1.95 (1H, m), 2.16–2.21 (2H, m), 2.93 (1H, m), 3.40 (1H, dd, 5.2, 9.2), 5.47 (1H, br d, 9.2); ^{13}C NMR (101 MHz, $CDCl_3$) δ_C: 136.2, 129.9, 128.5, 126.3, 47.5, 37.7, 33.8, 33.7, 28.8, 26.7, 26.3, 24.7, 17.9, 13.5, 12.2; GC-EIMS *m*/*z* 204 (100%), 189 (60%), 161 (57%), 147 (52%), 133 (45%), 119 (51%), 109 (56%), 107 (51%), 105 (69%), 91 (40%), 79 (22%), 67 (21%), 55 (18%), 41 (29%).

Calarene: Colorless oil; [α]20 D + 0.80 (*c* 0.125, ACN); UV (ACN) λ_{max} 207 nm; CD (*c* 1.00, ACN) λ(Δε) 216 (-1.39) nm; ^{1}H NMR (400 MHz, $CDCl_3$) δ_H (mult, *J* in Hz): 0.56 (1H, d, 9.2), 0.74 (1H, dt, 3.6, 9.6), 0.97 (3H, d, 6.8), 0.98 (3H, s), 1.01 (3H, s), 1.07 (3H, s), 1.34–1.45 (3H, m), 1.71–1.76 (2H, m), 1.92–2.01 (3H, m), 2.22 (1H, m), 5.24 (1H, br t, 2.4); ^{13}C NMR (101 MHz, $CDCl_3$) δ_C: 144.3, 120.5, 36.9, 36.8, 33.6, 30.1, 30.0, 27.4, 25.9, 23.1, 21.0, 19.7, 18.7, 16.7, 16.2; GC-EIMS *m*/*z* 204 (12%), 189 (18%), 161 (100%), 147 (13%), 133 (19%), 119 (28%), 105 (34%), 91 (19%), 79 (11%), 69 (11%), 53 (8%), 41 (16%).

β-Maaliene: Colorless oil; [α]20 D −0.48 (*c* 0.125, ACN); UV (ACN) λ_{max} 214 nm; CD (*c* 1.00, ACN) λ(Δε) 205 (-0.20) nm, 233 (+2.34) nm; ^{1}H NMR (400 MHz, $CDCl_3$) δ_H (mult, *J* in Hz): 0.73 (1H, t, 8.0), 0.84 (3H, s), 0.88–0.98 (3H, m), 0.99 (3H, s), 1.09 (3H, s), 1.16–1.22 (2H, m), 1.40 (1H, m), 1.56 (1H, m), 1.59 (3H, s), 1.61–1.66 (2H, m), 1.86–2.04 (2H, m); ^{13}C NMR (101 MHz, $CDCl_3$) δ_C: 131.8, 129.8, 38.7, 36.9, 32.5, 32.4, 29.3, 24.5, 24.3, 20.7, 19.9, 19.5, 18.1, 16.5, 15.6; GC-EIMS *m*/*z* 204 (85%), 189 (100%), 161 (100%), 147 (22%), 133 (56%), 119 (45%), 107 (30%), 105 (62%), 91 (40%), 79 (15%), 67 (15%), 55 (16%), 41 (28%).

2.4. GC–MS analysis

The GC–MS profiling was performed with an Agilent 7890B gas chromatography system equipped with an Agilent 7000D quadrupole mass spectrometry detector (Agilent Technologies, Santa Clara, CA, USA). Chromatographic separation was conducted on an HP-5MS quartz capillary column (30 m × 0.25 mm, 0.25 μm film thickness, 19091S-433, J&W Scientific, Folsom, CA, USA). Helium (99.999% purity) was used as the carrier gas at a 1.0 mL/min flow rate. The initial column temperature was 50°C, with heating to 150°C at 15°C /min, where it was kept for 3 min, followed by a rise at a rate of 2°C/min to 162°C, finally increasing at 20°C/ min to 250°C. The total running time was 20.667 min. The inlet temperature was held at 250°C with an injection volume of 1 μL sample solution and a split ratio of 1:10. The ion source (EI) and quadruple temperature were set at 230°C and 150°C, respectively, with a mass scanning range of 40–650 amu and an ionization voltage of 70 eV. The solvent delay time was established at 3.6 min to avoid the appearance of solvent peaks. Relative retention indices (RRI) against retention time were calculated using the same column with C_8–C_{40} as the reference standard and under the same operating conditions. Chemical constituents in volatile oil were characterized by matching the mass spectra to the spectra of reference compounds stored in the NIST 17.0 library, comparing their Kovats retention

indices against C_8–C_{40} *n*-alkanes, and comparing them with those reported in the literature. The relative contents of individual components were calculated in terms of GC peak area normalization without correction factors. Each essential oil determination was carried out in triplicate.

2.5. Animals

SPF grade C57BL/6 mice, male, 8 weeks, weight 18–22 g, were purchased from SPF (Beijing) biotechnology co., Ltd, housed in a barrier environment at the Animal Center of Tianjin University of Traditional Chinese Medicine, at 25°C and 50% humidity. The ventilation system was good, and the 12 h light and dark cycles were strictly maintained with food and water *ad libitum*. All experimental animal procedures were per the Regulations of the People's Republic of China on the Administration of Laboratory Animals. Prior to the start of the experiment, the mice were acclimatized for 7 days.

2.6. Evaluation of the vasodilatory activity

C57BL/6 mice (male, 8–10 weeks) were euthanized by isoflurane through inhalation. The thoracic aorta was removed and placed in Krebs-Henseleit (K-H) solution, including (mM): NaCl (118), $NaHCO_3$ (24.0), KCl (4.7), $MgSO_4{\cdot}7H_2O$ (1.2), KH_2PO_4 (1.8), $CaCl_2{\cdot}2H_2O$ (11.1), D-glucose (11). After carefully separating the excess tissue and fat around the thoracic aorta, the aorta was cut into 4 mm-length vascular rings. The aortic rings were placed in a bath at 37°C, 5 mL K-H solution, and continuously injected with a mixture of 95% O_2 + 5%CO_2 in a multi-channel *ex vivo* vascular tonometry system 630AM (Danish Myo Technology A/S, Denmark). Aortic rings were precontracted with 10^{-8} mol/L U46619. After the aortic rings reached their maximum contraction value, Ach (10^{-9}–10^{-5} mol/L) was added sequentially at 2 min intervals. Recording the diastolic curve, the endothelium of the aortic rings was intact if the maximum diastolic rate reached over 80%. The intact endothelium aorta was used to measure the vasorelaxation activity of the sample. After precontraction of the aortic rings with U46619, different concentrations of samples were added cumulatively at 5 min intervals. The relaxation rate was calculated using the following formula (Eq. (1)).

$$X\% = \frac{G_{U46619} - G_X}{G_{U46619} - G_0} \times 100\% \tag{1}$$

GU46619: maximum contractility due to U46619; G_X: contractility after 5 min of drug action; G_0: Resting contractility.

2.7. Modeling of the GC spectrum-vasodilatory activity relationship

GCA and PLSR were employed in the spectrum-effect relationship modeling between the relative contents (percentage, %) of forty-eight constituents in EONJ and the vasodilatory activity data of each EONJ utilizing Excel 2016 for Windows 10 and RStudio software, respectively. The average diastolic rate of each EONJ at the concentration of 300 μg/mL was taken into account due to considerable variability under this concentration, which is favorable for the discovery of the bioactive constituents. The combination of GCA and PLSR methods enabled a mutual verification of the spectrum-effect relationship analysis between pharmacodynamic indices and chromatographic peaks, enhancing the credibility of these efficacy-associated compounds selected out of the constituents in the volatile oils of *N. jatamansi*.

2.7.1. Gray correlation analysis (GCA)

GCA was conducted for the modeling of the spectrum-effect relationship utilizing Excel 2016. The data on the vasodilatory activities of the four EONJs served as reference sequences (parent sequences), and the data on the relative contents of forty-eight components obtained by GC–MS were treated as comparison sequences (sub-sequences) accordingly. Correlation coefficients (ξ_i) of the reference and comparison sequences derived from the GCA, representing the proximity of the associated factor sequence to the behavioral feature, were calculated using the mean value method. The higher the value ξ_i, the closer the sequence of correlation factors to the behavioral characteristics. The correlation degree (r) was obtained by calculating the mean value of the correlation coefficient between each indicator and the corresponding value of the reference sequence, which was designed to reflect the correlation between each evaluation object and the parent sequence (Chen et al., 2019; Huang et al., 2020; Xiao et al., 2018; Yuan et al., 2022; Zhang et al., 2019a). The contribution magnitude of each component to potency was assessed according to the ranking of the correlation degree, where r higher than 0.6 represented the existence of correlation while r greater than 0.8 reflected the high correlation (Chen et al., 2020; Yuan et al., 2022). The concrete calculation steps have been reported in detail in a published paper (Xiao et al., 2018).

Standardized processing of data (Eq. (2)):

$$\mathrm{X}_i(k) = \frac{X_i}{\sum_m^1 X}(i = 0, 1, 2, \cdots, \mathrm{n}; k = 1, 2, \cdots, \mathrm{m}) \tag{2}$$

$\mathrm{X}_0(k)$ denotes the reference sequence.

Calculation of correlation coefficients (ξ) (Eq. (3)):

$$\xi_i(k) = \frac{min_i min_k |X_0(k) - X_i(k)| + \rho max_i max_k |X_0(k) - X_i(k)|}{|X_0(k) - X_i(k)| + \rho max_i max_k |X_0(k) - X_i(k)|} \tag{3}$$

ρ represents the resolution coefficient, the smaller the ρ, the greater the resolution. ρ value range from 0 to 1, and it is taken as 0.5 in this work.

Calculation of correlation degree (r) (Eq. (4)):

$$r_{0i}(k) = \frac{1}{m}\sum_{k=1}^{m} \xi_{i(k)} \tag{4}$$

2.7.2. Partial least squares regression analysis (PLSR)

Partial least squares regression model between the vasodilatory activity and GC–MS spectrums was established to explore potential bioactive constituents utilizing RStudio. For this method, the X-matrix consisted of the relative content data of the individual constituents of the GC–MS spectrum. At the same time, the Y-matrix was composed of the vasorelaxant activity data of the four EONJs. It was followed by a regression procedure. More specifically, the two sets of data were standardized, and the regression was analyzed subsequently to obtain the regression coefficient (r') for the X variable rela-

tive to the Y variable. In the algorithm, a decomposition of the X variable predicts the Y variable. In contrast, the algorithm enables the discovery of several latent variables which can maximally explain the X variable and be correlated with the Y variable.

2.8. Network pharmacological workflow

2.8.1. Prediction of the drug-like properties and toxicological parameters

In this study, the chemical structures of the forty-eight phytochemicals identified from the four EONJs were retrieved or verified via several online databases such as PubChem (https://pubchem.ncbi.nlm.nih.gov), ChemSpider (https://www.chemspider.com) and Chemical Book (https://www.chemicalbook.com/ProductIndex.aspx), as well as the reported literature data on *N. jatamansi*. Their 2D structure drawing was accomplished by ChemDraw 19.0 software.

The SwissADME web tool (https://www.swissadme.ch) was employed to obtain the corresponding canonical SMILES coding of the compounds as well as the drug-like properties comprising molecular weight (MW), number of hydrogen bond donors (Hdon), number of hydrogen bond acceptors (Hacc), lipid-water partition coefficient (LogP) and number of rotatable bonds (Rbon). Lipinski rule, *viz*. Rule of Five (RO5, MW $\leq$ 500, Hdon $\leq$ 5, Hacc $\leq$ 10, LogP $\leq$ 5 and Rbon $\leq$ 10) (Yang et al. 2020; Zeng et al. 2022), was applied for the bioavailability evaluation based on the 2D structures of these compounds. Synthetic accessibility score (SAscore) was collected using the ADMETlab 2.0 database (https://admetmesh.scbdd.com), with SAscore greater than 6 indicating difficult synthesis and SAscore $<$ 6 representing easy synthesis (Zeng et al. 2022).

In addition, drug toxicology plays a critical role in preclinical investigations. Therefore, the toxicological parameters of the forty-eight compounds were calculated by the Protox II webserver (https://tox-new.charite.de/protox_II/) (for predicting the toxicity of chemicals) and the toxicological endpoints (hepatotoxicity, carcinogenicity, immunotoxicity, mutagenicity, cytotoxicity, and acute oral toxicity (LD_{50}, mg/kg) were in binary format reported as active or inactive. Finally, a graphic visualization was done utilizing the online bioinformatics website (https://www.bioinformatics.com.cn/).

2.8.2. Collection of predictive targets and CVD-associated targets

The PharmMapper (https://www.lilab-ecust.cn/pharmmapper/), SwissTarget Prediction (https://www.swisstargetprediction.ch/), TCMID (https://www.megabionet.org/tcmid/), TCMSP (https://tcmsp-e.com/) and SEA (https://sea.bkslab.org/) databases were chosen to predict the potential targets of the forty-eight constituents of EONJ. The OMIM (https://www.omim.org/), TTD (https://db.idrblab.net/ttd/), GeneCards (https://www.genecards.org/), DisGenet (https://www.disgenet.org/) and Drugbank (https://go.drugbank.com/) databases were retrieved for the possible targets concerning CVD by using the keyword 'cardiovascular disease'. Furthermore, the Uniprot database (https://www.uniprot.org/) was employed to translate the target names into the corresponding gene name. The collection and organization of the target information were completed by Microsoft Excel software (version 2016). Finally, the potential targets of the forty-eight phytochemicals were intersected with those related to CVD utilizing the Venn diagram to obtain the target proteins of EONJ-CVD.

2.8.3. Protein-Protein interaction (PPI) network

The PPI network of the compound targets for EONJ-CVD and EONJ was constructed by STRING database (https://string.embl.de/), with 'Organism' set to 'Homo sapiens', 'Minimum required interaction score' selected as 'medium confidence (0.400)', and the remaining parameters were left unchanged. Next, the interaction information was downloaded to be imported into Cytoscape software (v 3.7.1) for better optimization and visualization of the PPI network. Network Analyzer (a Cytoscape plugin) is applied to calculate the degree values and ranking. The color and size of the node correlate with its degree value. The larger the node's degree and the darker the color are, the higher the node's importance in the PPI network. Accordingly, the top core targets in the PPI network could be screened out.

2.8.4. Construction of 'EONJ-ingredients-target-CVD' network

Based on the protein interaction target data of EONJ and CVD, the active components of EONJ that could act on CVD were introduced, and 'EONJ-ingredients-common target-CVD' network diagrams were established by Cytoscape 3.7.1 software for visualizing. The network structure was analyzed by Network Analyzer with the node sorting and ranking based on degree value, and the potential active makers of EONJ against CVD were filtered. The Vertical Drop Line diagram, displaying the numbers of CVD-related targets targeted by the EONJ phytochemicals, was prepared using Origin 2021 software.

2.8.5. Pathway enrichment analysis

After the collection of the common targets of EONJ-CVD, Disease Ontology (DO) and Kyoto Encyclopedia of Genes and Genomes (KEGG) pathway enrichment analyses were performed with the DOSE, Bioconductor, and ClusterProfiler R packages. The top 20 DO, and KEGG terms sorted by gene count enriched were visualized by R 4.1.0 software. Cytoscape 3.7.1 was again deployed to construct 'target-pathway' networks. To further reveal the relationship among the biological functions, signal pathways involved in common targets, and their potential scientific connotations in biological networks, Gene Ontology (GO) functional enrichment, and KEGG pathway enrichment analyses were implemented using ClueGO plugin of Cytoscape widely utilized. Supplementarily, DO annotate genes based on human disease. GO analysis focuses on the biological process (BP) of the target. In contrast, KEGG pathway enrichment analysis was performed to probe the potential biological pathways related to the target.

2.9. Statistic analysis

The experimental results are presented by Mean $\pm$ SEM; Data comparisons between the two groups were independent of each other Sample T-test, multi-group comparison using one-way ANOVA. Values of $p < 0.05$ were considered statistically significant. Statistical analyses were performed using GraphPad Prism 8 and SPSS 21.0 Software.

3. Results

3.1. GC–MS profiling of the four EONJs

NJ-A, with an aromatic odor, was obtained as a pale yellow-green oily liquid (0.8 mL) from the dried rhizomes of *N. jatamansi* by hydro-distillation with a yield of 2.67% (*v*/*w*) above the limit requirement (1.8%) in the Chinese Pharmacopoeia (China Pharmacopoeia Committee, 2020b). The GC–MS total ion flow chromatograms (TIC) of the four EONJs are shown in Fig. 1. The corresponding identification results, including the retention time (RT), relative retention index (RRI), and the relative content of each constituent, are listed in Table 1.

A total of forty-eight compounds were identified, as shown in Fig. 1. The main components were sesquiterpenes, accounting for 77.08% of the numbers of the total components. At the same time, monoterpenes were also present in EONJ, representing about 22.92%. Among them, thirty-seven chemical constituents from NJ-A, forty chemical constituents from NJ-B, thirty-three chemical constituents from NJ-C, and thirty-eight chemical constituents from NJ-D were characterized, contributing to 91.89%, 92.78%, 95.23%, and 83.32% of the total essential oil, respectively. The main constituents in each essential oil of *N. jatamansi* were: NJ-A, calarene (19.47%), ledene oxide-(II) (12.13%), patchouli alcohol (11.36%), and maaliol (6.74%); NJ-B, calarene (35.15%), *β*-maaliene (9.54%), valerena-4,7(11)-diene (6.31%); NJ-C, *β*-maaliene (32.23%), calarene (25.74%), patchouli alcohol (6.23%), (-)-aristolene (6.13%); and NJ-D, valencene (12.51%), calarene (10.1%), guaia-6,9-diene (8.22%). Accordingly, calarene is one of the most predominant constituents of NJ-A, NJ-B, NJ-C, and NJ-D. This result is generally consistent with those reported (Liu and Liu, 2014; Maiwulanjiang et al., 2015; Wang et al., 2010).

The dendrogram depicted in Fig. 2 displayed the results of agglomerative hierarchical clustering analyses on the forty-eight compounds identified in the four EONJs. NJ-A and NJ-B fall into one cluster because of their high similarity in chemical composition and the relative content of each common constituent. NJ-C seems more alike to NJ-A and NJ-B compared to NJ-D, differing marginally in the contents of the common constituents. Among these EONJs, NJ-C contains the minimum number of constituents, while NJ-D possesses the largest number of constituents. NJ-D is quite different from other EONJs in chemical composition and the relative content of each common constituent. So, it could be speculated that NJ-D may originate from a different variety of *N. jatamansi* against those of other EONJs.

Overall, seventeen constituents, including calarene, *β*-maaliene, valerena-4,7(11)-diene, (-)-aristolene, seychellene, valencene, patchouli alcohol, maaliol, α-maaliene, (-)- globulol, (*E*)-*β*-caryophyllene, ledene oxide-(II), α-bulnesene, *γ*-himachalane, α-patchoulene, *β*-elemene, and *β*-patchoulene were found to be the major common constituents in EONJs, accounting for 69.53%, 79.31%, 89.27% and 47.28% of the whole chemical constituents of NJ-A, NJ-B, NJ-C, and NJ-D, respectively. Notably, bicyclosesquiphellandrene (4.39%), α-cadinol (3.92%), jatamansone (3.78%), and spirojatamol (2.74%) were prevalent ingredients of NJ-D, in which these constituents as aristolone, spathulenol, *trans*-*β*-ionone, and aromadendrene epoxide were absent instead. Guaia-6,9-diene could be detected at 0.88%, 0.22%, and 8.22% in NJ-A, NJ-B, and NJ-D, respectively, whereas it has not been detected in NJ-C. Further, there were great differences in the relative contents of those common constituents, including *β*-

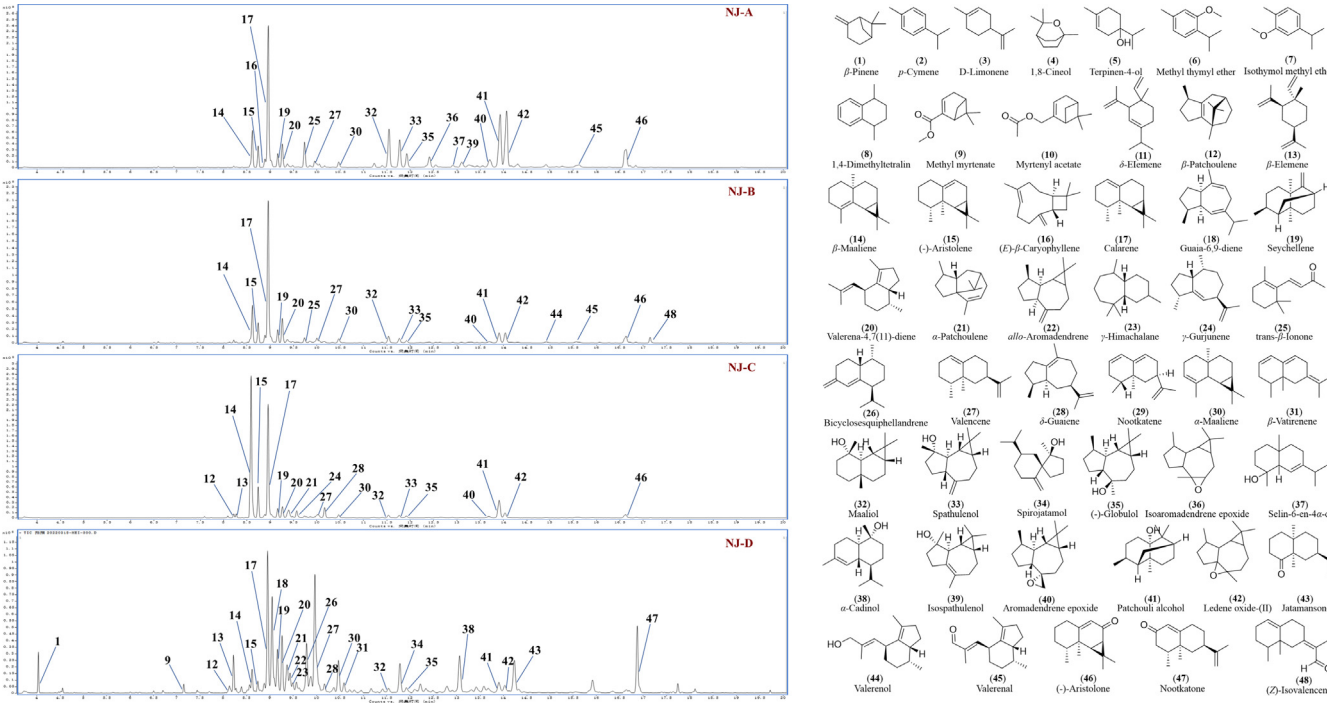

Fig. 1 Total ion chromatograms of EONJs and the chemical structures of forty-eight ingredients identified by GC–MS.

Table 1 Phytochemical identification of four EONJs based on GC–MS analysis.

No.	RT (min)	Compound	RRI[a]	RRI[L]	Formula	CAS No.	Percent (% peak area)			
							NJ-A	NJ-B	NJ-C	NJ-D
1	4.033	*β*-Pinene	/	979	$C_{10}H_{16}$	127–91-3	0.01	0.16	0.03	1.7
2	4.500	*p*-Cymene	1038	1023	$C_{10}H_{14}$	99–87-6	/	0.01	/	0.01
3	4.514	D-Limonene	1039	1029	$C_{10}H_{16}$	5989–27-5	/	0.02	0.01	0.09
4	4.554	1,8-Cineol	1043	1031	$C_{10}H_{18}O$	470–82-6	0.03	0.32	0.02	0.24
5	6.005	Terpinen-4-ol	1191	1177	$C_{10}H_{18}O$	562–74-3	0.01	0.03	/	0.06
6	6.506	Methyl thymyl ether	1245	1237	$C_{11}H_{16}O$	1017–56-8	0.04	0.09	0.01	0.1
7	6.602	Isothymol methyl ether	1255	1245	$C_{11}H_{16}O$	31574–44-4	0.11	0.26	0.03	0.02
8	6.930	1,4-Dimethyltetralin	1288	1283	$C_{12}H_{16}$	4175–54-6	0.11	0.05	0.02	0.03
9	7.150	Methyl myrtenate	1310	1301	$C_{11}H_{16}O_2$	30649–97-9	/	/	/	0.46
10	7.436	Myrtenyl acetate	1336	1326	$C_{12}H_{18}O_2$	1079–01-2	0.09	0.1	0.02	0.13
11	7.588	*δ*-EIemene	1349	1338	$C_{15}H_{24}$	20307–84-0	0.02	0.04	0.24	/
12	8.217	*β*-Patchoulene	1402	1380	$C_{15}H_{24}$	514–51-2	0.15	0.56	0.71	2.27
13	8.271	*β*-Elemene	1406	1389	$C_{15}H_{24}$	515–13-9	0.11	0.24	0.73	0.3
14	8.616	*β*-Maaliene	1429	1415	$C_{15}H_{24}$	489–29-2	4.76	9.54	32.23	1.68
15	8.743	(-)-Aristolene	1438	1429	$C_{15}H_{24}$	87–44-5	2.56	4.63	6.13	0.85
16	8.886	(*E*)-*β*-Caryophyllene	1447	1440	$C_{15}H_{24}$	154098–14-3	1.06	1.83	0.85	0.86
17	8.954	Calarene	1451	1430	$C_{15}H_{24}$	17334–55-3	19.47	35.15	25.74	10.1
18	9.045	Guaia-6,9-diene	1457	1451	$C_{15}H_{24}$	36577–33-0	0.88	0.22	/	8.22
19	9.16	Seychellene	1464	1446	$C_{15}H_{24}$	20085–93-2	1.78	3.24	2.11	3.6
20	9.257	Valerena-4,7(11)-diene	1470	1456	$C_{15}H_{24}$	351222–66-7	3.16	6.31	2.75	4.26
21	9.366	α-Patchoulene	1477	1467	$C_{15}H_{24}$	560–32-7	0.76	1.49	3	2.89
22	9.43	*allo*-Aromadendrene	1481	1465	$C_{15}H_{24}$	125135–08-2	/	/	/	1.65
23	9.489	*γ*-Himachalane	1484	1480	$C_{15}H_{28}$	53111–25-4	0.34	0.49	0.32	0.92
24	9.568	*γ*-Gurjunene	1489	1477	$C_{15}H_{24}$	22567–17-5	/	0.34	1.91	1.03
25	9.735	*trans*-*β*-Ionone	1499	1488	$C_{13}H_{20}O$	79–77-6	3.51	1.65	0.55	/
26	9.784	Bicyclosesquiphellandrene	1502	1495	$C_{15}H_{24}$	54324–03-7	/	/	/	4.39
27	9.963	Valencene	1511	1496	$C_{15}H_{24}$	4630–07-3	1.51	1.82	1.71	12.51
28	10.167	*δ*-Guaiene	1521	1510	$C_{15}H_{24}$	3691–11-0	0.26	0.48	2.65	0.95
29	10.368	Nootkatene	1531	1511	$C_{15}H_{22}$	5090–61-9	/	/	/	0.65
30	10.466	α-Maaliene	1536	1522	$C_{15}H_{24}$	489–28-1	0.94	1.46	0.88	3.03
31	10.585	*β*-Vatirenene	1541	1540	$C_{15}H_{22}$	27840–40-0	0.05	0.02	/	0.95
32	11.537	Maaliol	1584	1574	$C_{15}H_{26}O$	527–90-2	6.74	2.45	0.81	0.46
33	11.777	Spathulenol	1595	1577	$C_{15}H_{24}O$	6750–60-3	4.79	1.78	0.76	/
34	11.786	Spirojatamol	1595	1585	$C_{15}H_{26}O$	128487–46-7	/	/	/	2.74
35	11.929	(-)-Globulol	1601	1590	$C_{15}H_{26}O$	489–41-8	2.44	0.91	0.62	0.36
36	12.411	Isoaromadendrene epoxide	1620	1610	$C_{15}H_{24}O$	/	2.1	0.44	0.12	/
37	12.915	Selin-6-en-4α-ol	1639	1636	$C_{15}H_{26}O$	118173–08-3	0.5	0.2	0.11	/
38	13.064	α-Cadinol	1645	1653	$C_{15}H_{26}O$	481–34-5	/	/	/	3.92
39	13.105	Isospathulenol	1646	1638	$C_{15}H_{24}O$	88395–46-4	1.25	0.24	/	/
40	13.707	Aromadendrene epoxide	1668	1672	$C_{15}H_{24}O$	85710–39-0	2.13	0.78	0.62	/
41	13.909	Patchouli alcohol	1675	1663	$C_{15}H_{26}O$	5986–55-0	11.36	4.17	6.23	1.28
42	14.070	Ledene oxide-(II)	1680	1631	$C_{15}H_{24}O$	/	12.13	4.54	1.8	0.96
43	14.238	Jatamansone	1686	1675	$C_{15}H_{26}O$	1803–39-0	/	/	/	3.78
44	14.915	Valerenol	1712	1736	$C_{15}H_{24}O$	101628–22-2	0.66	0.77	0.14	/
45	15.553	Valerenal	1738	1720	$C_{15}H_{22}O$	4176–16-3	1.11	0.71	/	0.17
46	16.629	Aristolone	1781	1763	$C_{15}H_{22}O$	6831–17-0	4.87	3.49	1.37	/
47	16.875	Nootkatone	1790	1806	$C_{15}H_{22}O$	4674–50-4	/	/	/	5.7
48	17.245	(*Z*)-Isovalencenal	1800	1812	$C_{15}H_{22}O$	137695–20-6	0.09	1.75	/	/
	Total (%)						91.89	92.78	95.23	83.32
	Monoterpene hydrocarbons						0.12	0.24	0.06	1.83
	Oxygenated monoterpenes						3.79	2.45	0.63	1.01
	Total monoterpenoids						3.91	2.69	0.69	2.84
	Sesquiterpene hydrocarbons						37.81	67.86	81.96	59.30
	Oxygenated sesquiterpenes						50.17	22.23	12.58	21.18
	Total sesquiterpenoids						87.98	90.09	94.54	80.48

RRI[a], Relative retention index calculated against homologous series of alkanes (C_8–C_{40}) on HB-5MS capillary column.
RRI[L], Relative retention index reported in the literature about GC–MS analysis.by HB-5MS capillary column.

maaliene, valencene, patchouli alcohol, ledene oxide-(II), (-)-aristolene, and maaliol among the four EONJs. This phenomenon illustrated that the composition of EONJ varies greatly in type and content depending on the origin. The chemical profile of EONJ is susceptible to those changes in growing, collecting, storage, and processing conditions, prompting us to conduct an urgent future study on the global quality control of EONJs and their processed products.

3.2. Vasodilatory activity induced in mice aorta rings by four EONJs

Aortic rings were contracted with U46619 (10^{-8} mol/L), and vasodilator responses were measured with four EONJs added at different final concentrations (50, 150, 300, 500, and 750 μg/mL). As shown in Table 2 and Fig. 3, the vasoconstriction caused by U46619 could be significantly relaxed after the treatment of four EONJs compared to the Veh group. NJ-A, NJ-B, NJ-C, and NJ-D exhibited similar significant vasodilatory activity with EC_{50} values of 350.1 μg/mL, 251.3 μg/mL, 210.4 μg/mL, and 292.2 μg/mL, respectively. The mean relaxation rates of the four EONJs at 300 μg/mL were used as the representative vasodilatory data for further study of the chromatographic spectrum-vasodilatory activity relationship, aiming to facilitate the preliminary discovery of vasodilatory contribution ingredients.

3.3. Analysis of the spectrum-effect relationship by GCA and PLSR models

In this experiment, spectrum-effect relationship models were established between the GC–MS spectrum (*viz*. TIC chromatographic relative contents of the forty-eight constituents) and the vasorelaxant activities of 300 μg/mL EONJs by two means of chemometrics (GCA and PLSR).

The GCA result was illustrated in Table S1 and Fig. 4A. Correlation degrees (r) of the identified peaks to the vasodilatory efficacy were between 0.5371 and 0.8571. Specifically, there were thirty-five components, each with a correlation degree above 0.6, indicating that most of the components of EONJ possess high relevance to the whole vasorelaxant efficacy of EONJ, and the vasodilatory effect of EONJ may be the comprehensive activity of those ingredients with high relevance. Herein, a correlation degree of 0.65 was taken as the cut-off. Twenty-eight peaks with high contribution were accordingly screened out, including P2, P5, P6, P7, P8, P10, P12, P13, P14, P15, P16, P17, P19, P20, P21, P23, P24, P25, P28, P30, P32, P33, P35, P37, P40, P41, P42, and P45.

Further, the PLSR result was shown in Table S2 and Fig. 4B. Correlation coefficient (r') of the forty-eight peaks to the vasodilatory efficacy was in a range of -0.0680 and 0.0674 (Fig. 4B). Among them, seventeen peaks (P2, P4, P7, P11, P12, P13, P14, P15, P16, P17, P19, P20, P21, P24, P28, P41, and P48) showed positive correlations with the vasodilatory activity. In contrast, the remaining peaks exhibited negative ones. It can be speculated that these seventeen components may exert beneficial perturbation for the vasodilatory activity of EONJ. Among them, ten peaks (P11, P13, P14, P15, P17, P21, P24, P28, P41, and P48) were selected due to their significant contributions in the correlation coefficients ranked by magnitude.

Based on the above-mentioned GCA and PLSR analytical results, eight relevant phytoconstituents, including β-elemene (P13), β-maaliene (P14), (-)-aristolene (P15), calarene (P17), α-patchoulene (P21), γ-gurjunene (P24), δ-guaiene (P28) and patchouli alcohol (P41), were finally selected out as the key facilitators of vasodilatory activity. Interestingly, β-maaliene (P14), (-)-aristolene (P15), calarene (P17), and patchouli alcohol (P41) have been previously reported as the major active constituents with high relative contents in EONJs (Bose et al., 2019; Geng et al., 2011; Tanaka and Komatsu, 2008; Wang et al., 2010), which meet, to some extent, the principle of consistency of content-potency and are expected to be selected as the biomarkers for quality control of EONJs.

3.4. Network pharmacology

3.4.1. Drug-like properties and toxicological parameters of the 48 EONJ ingredients

The 2D structures of the forty-eight phytochemical constituents were presented in Fig. 1. The SMILES for their structures were specifically collated (Table S3) and used for

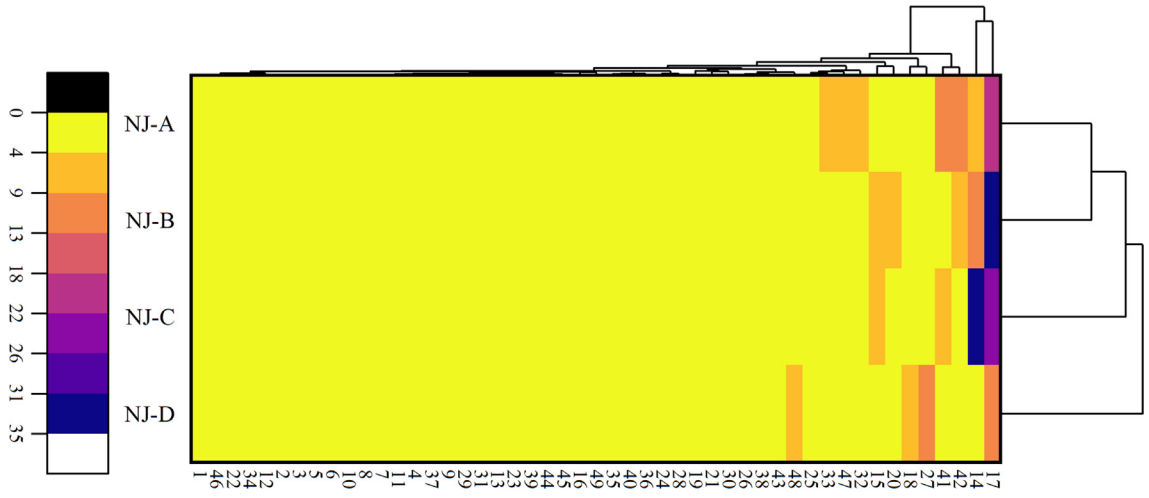

Fig. 2 Agglomerative hierarchical clustering analysis of the ingredients of four EONJs based on GC–MS data.

Table 2 Vasodilatory activities of the four EONJs.

Essential oil	Relaxation (%)					EC_{50} (μg/mL)
	50 μg/mL	150 μg/mL	300 μg/mL	500 μg/mL	750 μg/mL	
NJ-A	-0.88 ± 3.14	7.36 ± 5.59	35.53 ± 2.29**	73.76 ± 3.39***	92.32 ± 3.11***	350.1
NJ-B	4.71 ± 1.24	23.71 ± 4.35**	52.25 ± 5.47***	77.88 ± 4.74***	90.11 ± 3.01***	251.3
NJ-C	2.67 ± 2.78	22.12 ± 2.09**	61.16 ± 3.97***	90.55 ± 5.69***	92.82 ± 4.54***	210.4
NJ-D	2.22 ± 0.26	19.33 ± 1.95**	46.80 ± 3.19***	74.00 ± 3.60***	88.05 ± 2.57***	292.2

n = 3,**p < 0.01 *vs.* Veh., ***p < 0.001 *vs.* Veh., The vehicle group (Veh) was treated with an equal volume of DMSO.

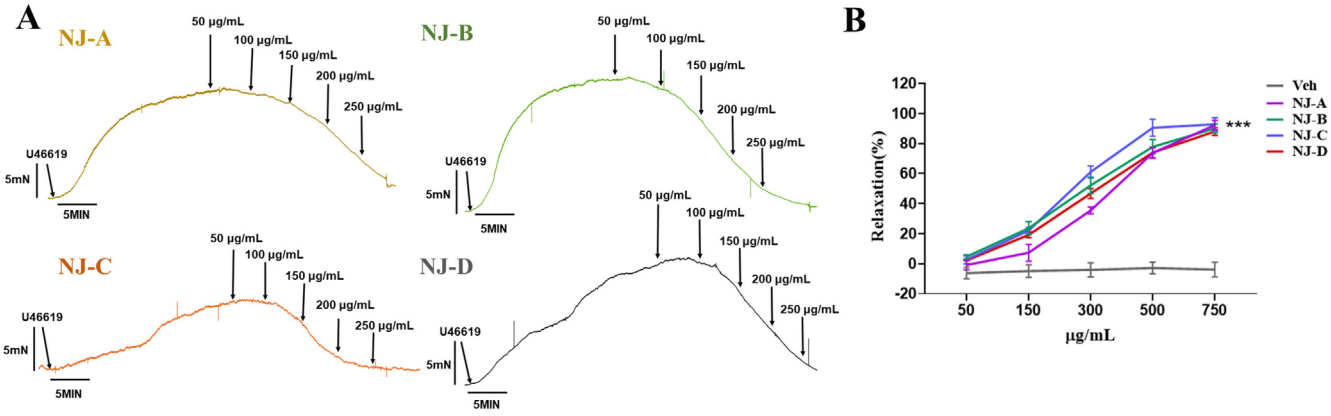

Fig. 3 Vasodilatory activity of the four EONJs (A) The representative tracing of aortic ring relaxation for four EONJs; (B) The line graph of vasodilatory activity on four EONJs (n = 3. ***p < 0.001 *vs.* Veh.).

simulating their drug-like properties (RO5 and SAscore), as listed in Table S4. The results indicated that all these forty-eight compounds conformed to the RO5 principle. Their simulated SAscore values were all less than 6 as they may be relatively easier to synthesize. Hence, these forty-eight phytochemicals of EONJs were all selected for the subsequent investigations.

Firstly, in view of the vital role of potential toxicological properties or possible side effects of the major phytoconstituents in the field of preclinical development for herbal medicines, toxicological parameters of the above forty-eight constituents were calculated, as shown in Table S5. As shown in Fig. S10, the result revealed that none of the EONJ phytochemicals turned out to be hepatotoxic or cytotoxic. However, (-)-aristolene, (*E*)-*β*-caryophyllene, calarene, bicyclosesquiphellandrene, spirojatamol, selin-6-en-4*α*-ol, *α*-cadinol, and isospathulenol were figured out to be immunotoxic, 1,4-dimethyltetralin tended to be mutagenic. At the same time, *p*-cymene, methyl thymyl ether, and isothymol methyl ether seemed to be carcinogenic.

3.4.2. Prediction and collection of the potential targets

As illustrated in Fig. 5, a total of 319 potential targets of EONJ constituents were finally collated by integrating the 130, 77, 89, 113, and 76 predictive targets from PharmMapper, SwissTarget Prediction, TCMID, TCMSP, and SEA databases, respectively. And 1461 CVD-associated targets were afforded by combining the 680, 65, 510, 358, and 95 targets obtained from OMIM, TTD, GeneCards, DisGenet, and Drugbank databases, respectively. Finally, 63 common targets were screened out through the intersection of the EONJ constituents' predictive targets and the CVD-associated targets.

3.4.3. DO enrichment analysis of the 319 predictive targets

DO functional enrichment was further conducted to evaluate the relevance of the 319 constituents' predictive targets to human diseases, resulting in the enrichment of a total of 405 DO terms. As depicted in Fig. 6, the most prominent DO terms were obesity (DOID: 9970), overnutrition (DOID: 654), nutrition disease (DOID: 374), tauopathy (DOID: 680), Alzheimer's disease (DOID: 10652), coronary artery disease (DOID: 3393), brain disease (DOID: 936), myocardial infarction (DOID: 5844), a developmental disorder of mental health (DOID: 0060037), autism spectrum disorder (DOID: 0060041), autistic disorder (DOID:12849), arteriosclerotic cardiovascular disease (DOID: 2348), atherosclerosis (DOID:1936), etc. The detailed information of the top 20 DO terms enriched significantly is listed in Table S6. The top-enriched DO terms were mainly brain diseases, cardiovascular diseases, and obesity. Specifically, there were 46 targets for coronary artery disease, 40 for myocardial infarction, 39 for arteriosclerotic cardiovascular disease, and 39 for arteriosclerosis. As is well known, obesity and overnutrition are the major risk factors for various metabolic disorders and cardiovascular diseases (Lovren et al., 2015). This, to some extent, was consistent with those reported pharmacological activities of *N. jatamansi* (Bhat and Malik, 2020; Saroya and Singh, 2018), as summarized in our previously published review

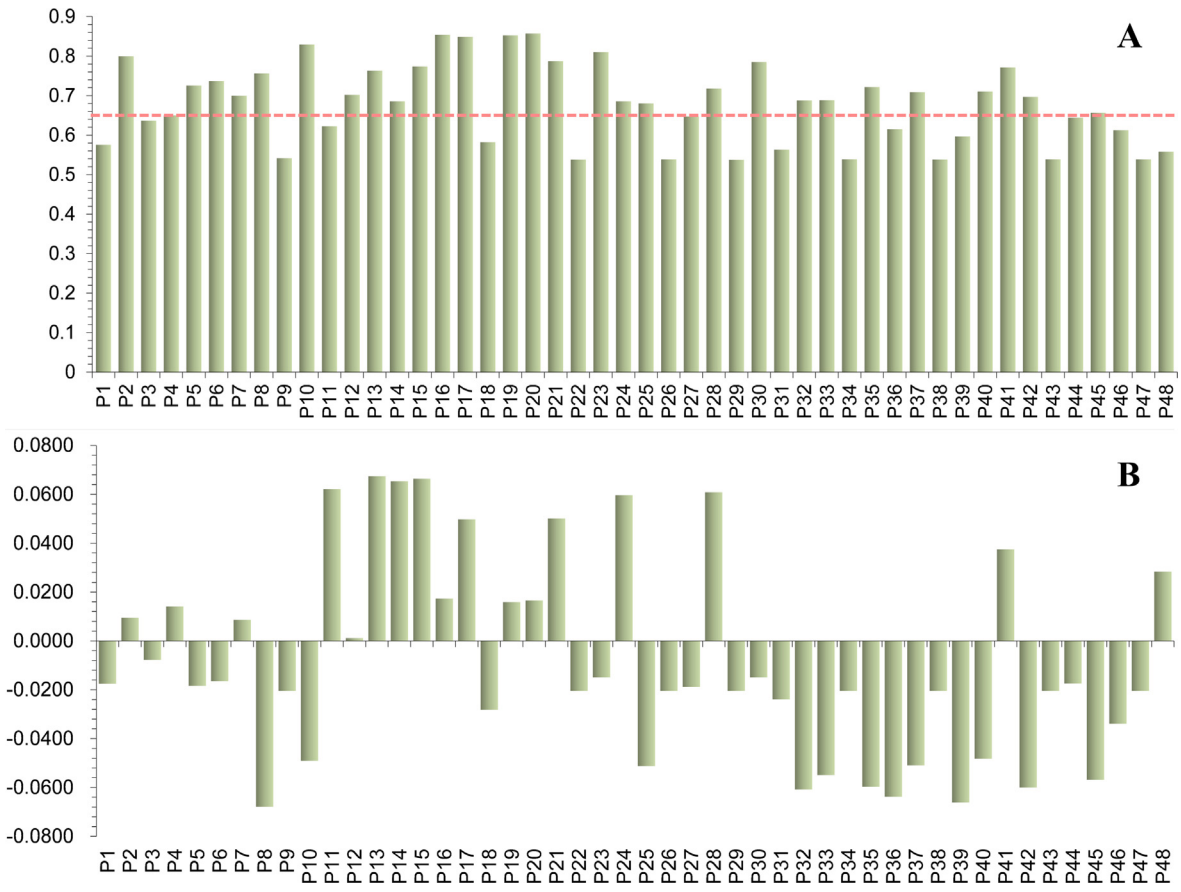

Fig. 4 The GCA and PLSR plots of the relationship between the GC–MS spectrum and the vasodilatory activities of EONJs (A) Grey correlation degree plot of each constituent to the vasodilatory efficacy (GCA); (B) Regression coefficient plot of each constituent to the vasodilatory efficacy (PLSR).

(Wang et al., 2021) that *N. jatamansi* has been prescribed in ethnic medical systems of different countries mainly for neurological, digestive, cardiovascular, and epidermal disorders.

3.4.4. Screening of the key targets

As shown in Fig. 7A–B, the PPI network was constructed for the 319 predictive targets of EONJ, among which the top 15 core targets were ALB, MAPK3, IL1B, SRC, EGFR, ESR1, PPARG, CASP3, HIF1A, PTGS2, MAPK1, MAPK14, PPARA, NOS3, and SLC6A4. Similarly, the PPI network of the 63 common targets between EONJ and CVD was established with 63 nodes and 361 edges, as presented in Fig. 7C–D, while the top 10 core targets were ALB, IL1B, PPARG, MAPK3, NOS3, CASP3, EGFR, PPARA, PTGS2, and HIF1A. It is worth mentioning that the numbers in red, shown in the bar chart of Fig. 7D, represented the degree ranking of the core targets in the PPI network of the 319 EONJ's predictive targets. Combining the analysis results of the two PPI networks mentioned above, ten key targets were screened out, including ALB, IL1B, PPARG, MAPK3, CASP3, EGFR, PTGS2, NOS3, PPARA, and HIF1A.

Some identified cardiovascular diseases, such as hyperlipidemia, hypertension, and diabetes, could increase the production of ROS and decrease the generation of endothelial NO. Under physiological conditions, NOS3, one of the endothelial nitric oxide synthases (eNOS), can synthesize NO, an essential vasoprotective factor of the endothelium. NOS3 plays a vital role in the treatment of CVD (Forstermann et al., 2017). PTGS2, as a cyclooxygenase, was proven to be a core gene in human coronary atherosclerosis. This may be attributed to the fact that cyclooxygenase affects the production of prostaglandins in response to increased oxidative stress and thereby affects vascular tone (Zhao et al., 2021; Zhou et al., 2021). Thus, NOS3 and PTGS2 were selected as the crucial targets because of their high relevance to hypertension.

By the way, as shown in Fig. 7E, the major constituents of EONJ, including aristolone (19 targets), β-patchoulene (18 targets), isospathulenol (15 targets), valencene (15 targets), calarene (15 targets), β-maaliene (15 targets), nootkatone (14 targets), patchouli alcohol (13 targets), α-maaliene (13 targets), (-)-aristolene (13 targets) and *p*-cymene (13 targets), occupy the largest number of targets. Considering the high relative contents, the satisfactory performance in the abovementioned spectrum-effect relationship analyses, and the attractive drug-like properties, the four major ingredients (β-maaliene, (-)-aristolene, calarene, and patchouli alcohol) were considered as the candidate active ingredients.

3.4.5. The 'EONJ-ingredients-targets-CVD' network

Based on the above-analyzed data, an 'EONJ-ingredients-targets-CVD' network concerning 48 ingredients and their relative targets was constructed (Fig. 8), resulting in 113 nodes

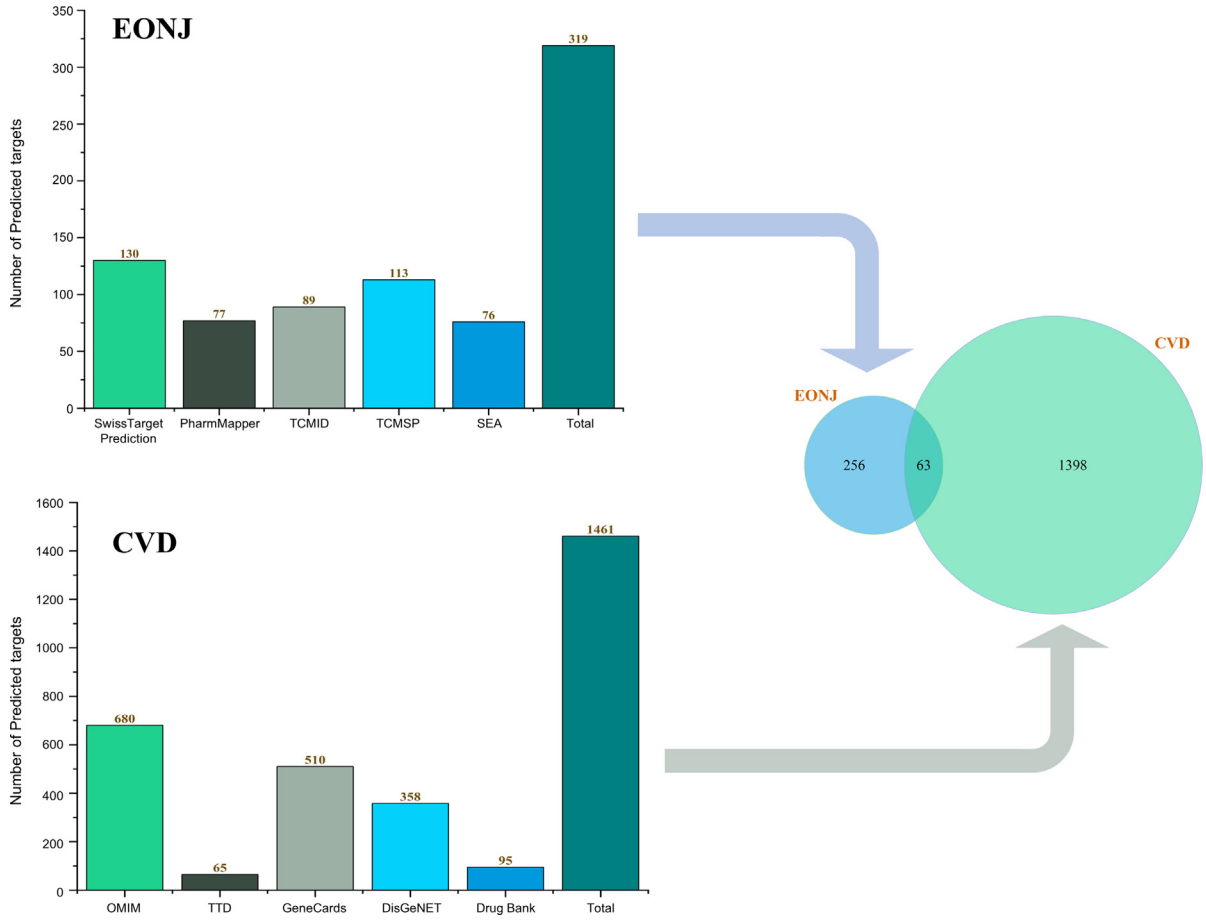

Fig. 5 Number of EONJ's predictive targets and CVD-associated targets.

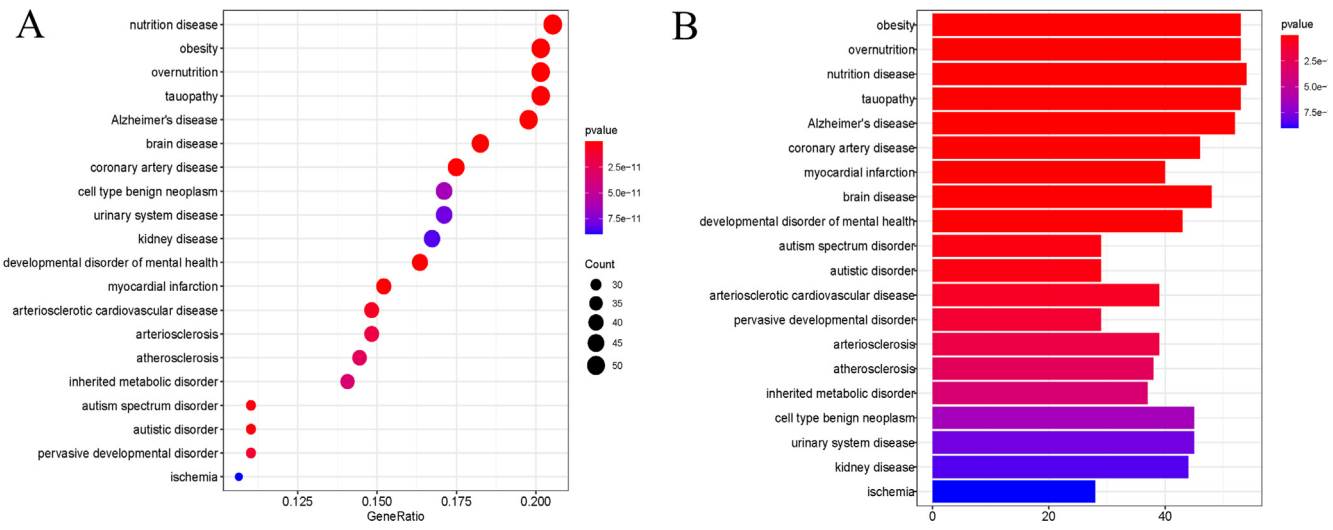

Fig. 6 The bubble diagram and bar chart on the top 20 significantly enriched Disease Ontology (DO) terms (A) Bubble diagram; (B) Bar chart (DO terms with corrected *p*-value < 0.05 were considered significantly enriched; GeneRatio of the x-axis represents the ratio of targets in the background terms; Bubble size represents the number of genes enriched; Bubble color represents *p*-value).

and 539 edges. Potential active ingredients and targets of EONJ are shown in different shapes and colors. Blue circles represent phytochemical ingredients, and green diamonds represent common targets between EONJ and CVD. And the edge represents the correlation among EONJ, active ingredients, targets, and CVD. Some of the target nodes, including ALB, CYP19A1, AR, PPARA, ESR1, ITGAL, MAPK1, and ESR2, appeared larger due to their larger degree values,

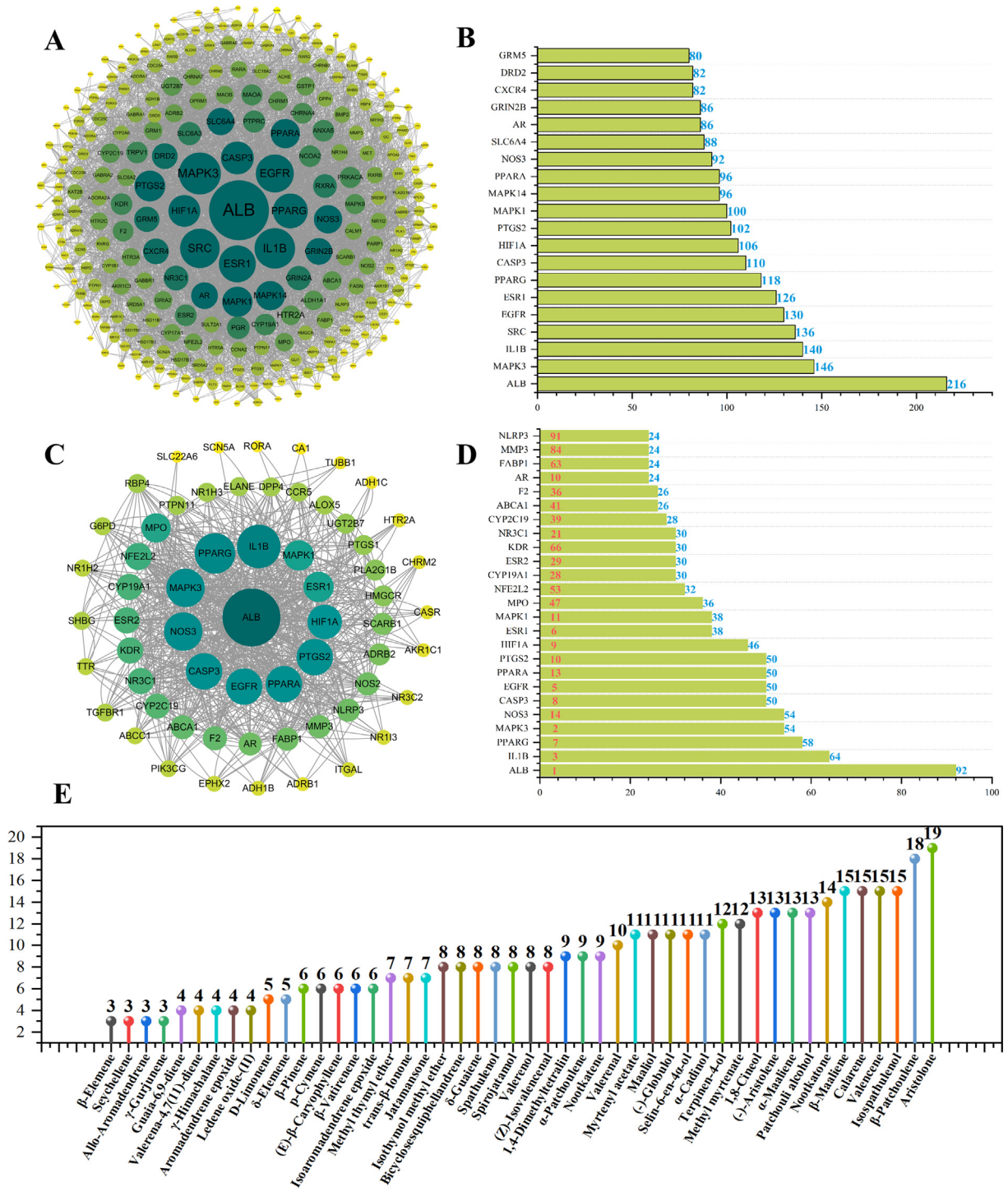

Fig. 7 The screening of core targets and bioactive phytochemicals. (A) The PPI network of 319 targets associated with 48 phytochemicals of EONJ; (B) The top 20 targets ranked by degree value were identified as the core targets related to EONJ; (C) The PPI network of 63 common targets between EONJ and CVD; (D) The top 25 targets ranked by degree value were classified as the core targets related to EONJ and CVD; (E) The vertical drop line diagram on 48 ingredients of EONJ and the numbers of their targets associated with CVD.

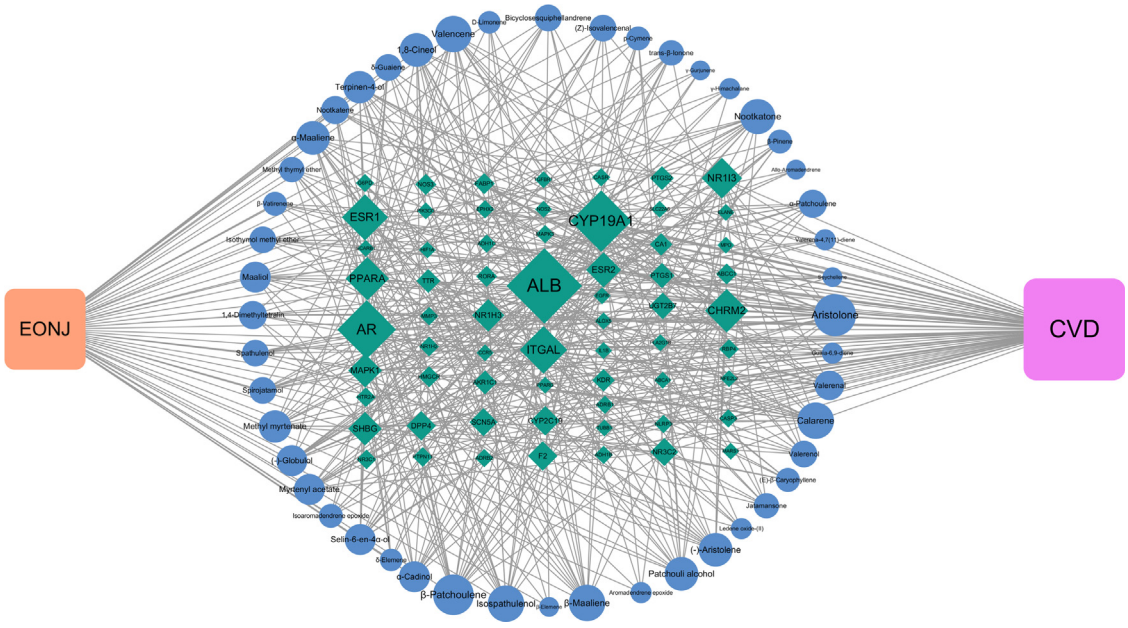

Fig. 8 'EONJ-ingredients-targets-CVD' network.

suggesting that these targets are more likely to be targeted by most of the EONJ ingredients.

3.4.6. GO enrichment and KEGG pathway analysis of the 63 common targets

GO enrichment and KEGG pathway analysis were further conducted for the 63 common targets. GO enrichment revealed the existence of 92 GO terms related to biological processes (BP) with 136 GO terms connections (Fig. 9), demonstrating that the main biological functions enriched include the positive regulation of vasoconstriction, nuclear receptor activity, regulation of cardiac muscle tissue growth, regulation of blood vessel endothelial cell migration, positive regulation of lipid biosynthetic process, positive regulation of the fatty acid metabolic process, positive regulation of prostaglandin biosynthetic process, response to lipopolysaccharide, regulation of MAP kinase activity, regulation of protein secretion, regulation of biomineral tissue development and the diterpenoid metabolic process, as well as some other biological processes.

As displayed in Fig. 10A and Table S7, the KEGG pathway analysis revealed that the main pathways involved were chemical carcinogenesis-receptor activation, serotonergic synapse, lipid and atherosclerosis, arachidonic acid metabolism, toxoplasmosis, etc. On the other hand, the 63 common candidate targets were further imported into the Clue GO plugin to carry out KEGG pathway analysis. As shown in Fig. 10B, the main pathways involved could be screened out, including chemical carcinogenesis, lipid and atherosclerosis, serotonergic synapse, PPAR signaling pathway, regulation of lipolysis in adipocytes, fat digestion and absorption, and ovarian steroidogenesis. The results showed us that the chemical carcinogenesis, lipid and atherosclerosis, and serotonergic synapse pathways might play vital roles in the treatment of EONJ against CVD. EONJ may exert its effects through multiple signaling pathways. The network diagram of co-targets involved in the top 20 KEGG pathways was presented in Fig. 11.

3.5. Vasodilatory activities of four available major EONJ constituents

Four available major EONJ constituents, including valerena-4,7(11)-diene, calarene, *β*-maaliene, and patchouli alcohol, were furtherly subjected to the abovementioned vascular tone test to evaluate their vasodilatory activities. As shown in Fig. 12 and Table 3, the result turned out that patchouli alcohol exhibited excellent vasodilatory activity with an EC_{50} value of 51.75 μg/mL. In contrast, *β*-maaliene possessed weak vasodilatory activity at 180 μg/mL and 380 μg/mL of high concentration. And other two constituents (calarene and valerena-4,7(11)-diene) could not significantly relax the vasoconstriction caused by U46619 compared to the Veh group.

4. Discussion

This work employed two spectrum-effect relationship models and a network pharmacological approach to identify the effective constituents in EONJ for combating CVD. The ultimate aim was to determine both the multi-target therapeutic potential and the molecular mechanisms involved. The screening process led to the identification of two significant bioactive compounds, patchouli alcohol, and *β*-maaliene, as well as two crucial targets, NOS3 and PTGS2, that make EONJ a potential treatment for CVD.

According to previous studies, patchouli alcohol, a calcium antagonist, has been shown to have significant vasodilatory effects via an endothelial non-dependent pathway (Hu et al., 2018), which corroborates the findings of this study. However, there is no evidence to suggest that *β*-maaliene, (-)-aristolene, or calarene have therapeutic benefits against hypertension. Instead, these compounds have significant sedative effects (Takemoto et al., 2008; Takemoto et al., 2009), which are commonly prescribed for prehypertension, stage I hypertension, and stage II hypertension (Parr et al., 2012). Thus, it is possible

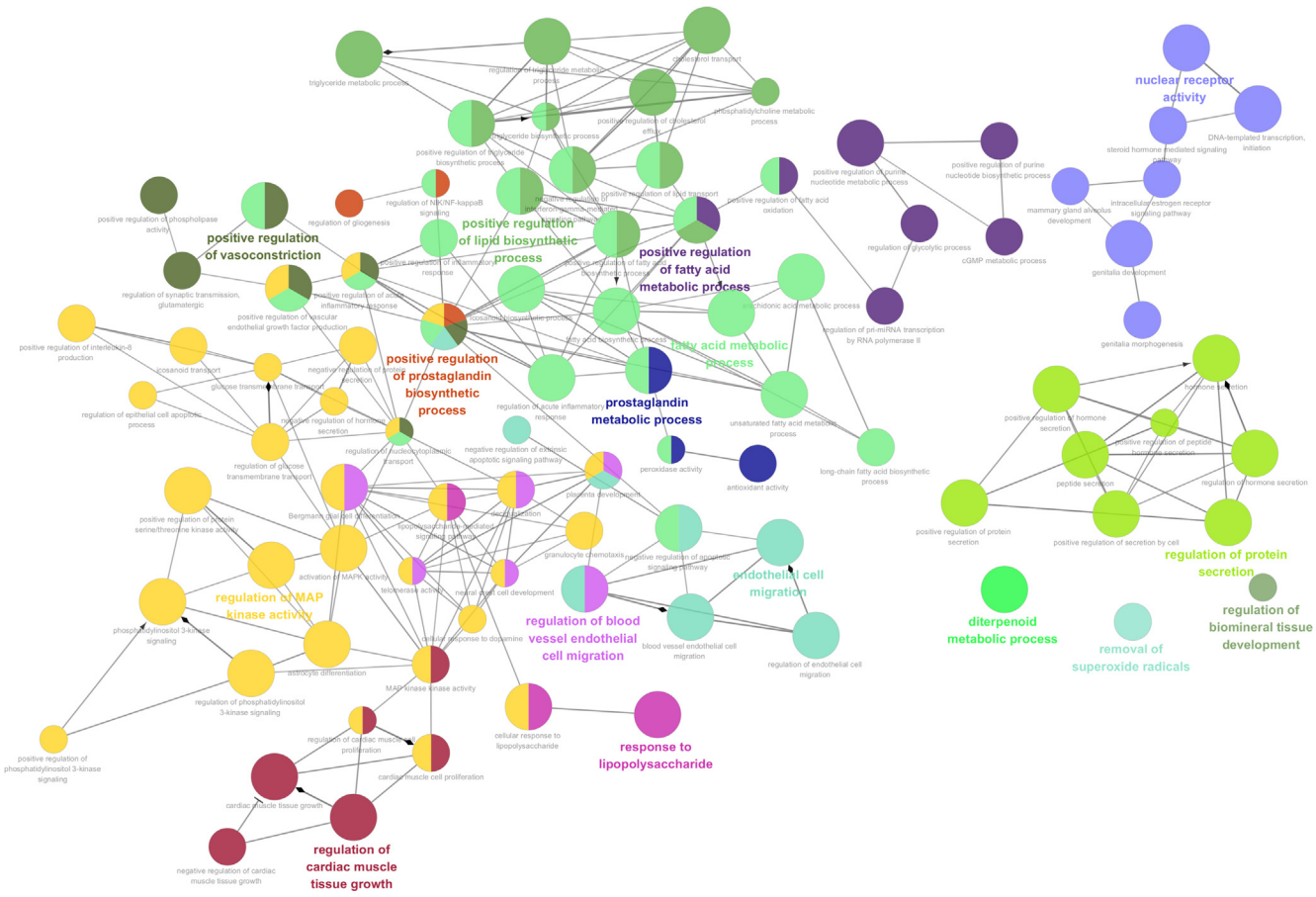

Fig. 9 The network plot shows biological processes of GO enrichment analysis (Each node indicates the enriched GO function term, the more significant the *p*-value is, the larger the node is; different colors represent different functional groups, the bold font is treated as the functional representation, and the line between nodes means the correlation among functions, and the diamond arrow refers to the regulatory effect, the triangular arrow shows the positive regulation).

that *β*-maaliene, (-)-aristolene, calarene, and valerena-4,7(11)-diene could aid in the prevention and treatment of hypertension. Interestingly, *β*-maaliene, (-)-aristolene, and calarene share an aristolane-like sesquiterpenoid scaffold, suggesting that they may be biosynthetic precursors or natural substrates before natural oxidation. This is important because (-)-aristolone and kanshone H, which have been found to have significant vasodilatory effects in alleviating hypertension, are derived from such oxidation (Fang et al., 2022). Therefore, it is worth exploring whether exposing EONJ to air for a certain period of time would lower blood pressure or enhance its vasodilatory effects. Further research is needed to determine whether the major ingredients in EONJ have a synergistic effect in relaxing blood vessels.

To further analyze the relationship between the relative contents of normalized common peak areas and the corresponding vasodilatory activity data, Pearson correlation coefficients were obtained using Origin 2021 software. As shown in Figure S11, red points indicate a positive correlation, while blue points indicate a negative correlation. P41 represents patchouli alcohol, and RR represents vasodilation rate. The result of the Pearson correlation analysis was consistent with the findings of the partial least squares regression (Fig. 4B). Several peaks (P11, P13, P14, P15, P17, P21, P24, P28, P41) were found to have significant positive correlations with EONJ's vasodilatory activity, suggesting that these constituents may have a beneficial impact on vasodilation. Furthermore, the Pearson correlation analysis revealed correlations among the 48 ingredients, indicating that there might be a synergistic effect among the volatile ingredients in EONJ.

Our investigation into the potential benefits of *N. jatamansi* led to the discovery that the herb's compounds may have the ability to regulate the activities of two enzymes: endothelial nitric oxide synthase (NOS3 or eNOS) and cyclooxygenase 2 (PTSG2 or COX-2), as revealed by our network pharmacology analysis. NOS3 produces nitric oxide, which aids in the relaxation of vascular smooth muscles and improves blood flow through a cGMP-mediated signal transduction pathway (Forstermann et al., 2017). PTGS2 is an inducible enzyme that produces prostanoids, enhancing vasodilation and preventing blood clots (Zhao et al., 2021; Zhou et al., 2021). Therefore, we propose that the herb's compounds could promote or induce the activity of these two enzymes, leading to enhanced vasodilation.

The KEGG analysis conducted in our study indicated significant enrichment of the lipid and atherosclerosis signaling pathways (Fig. S12). The PI3K and AKT proteins are essential

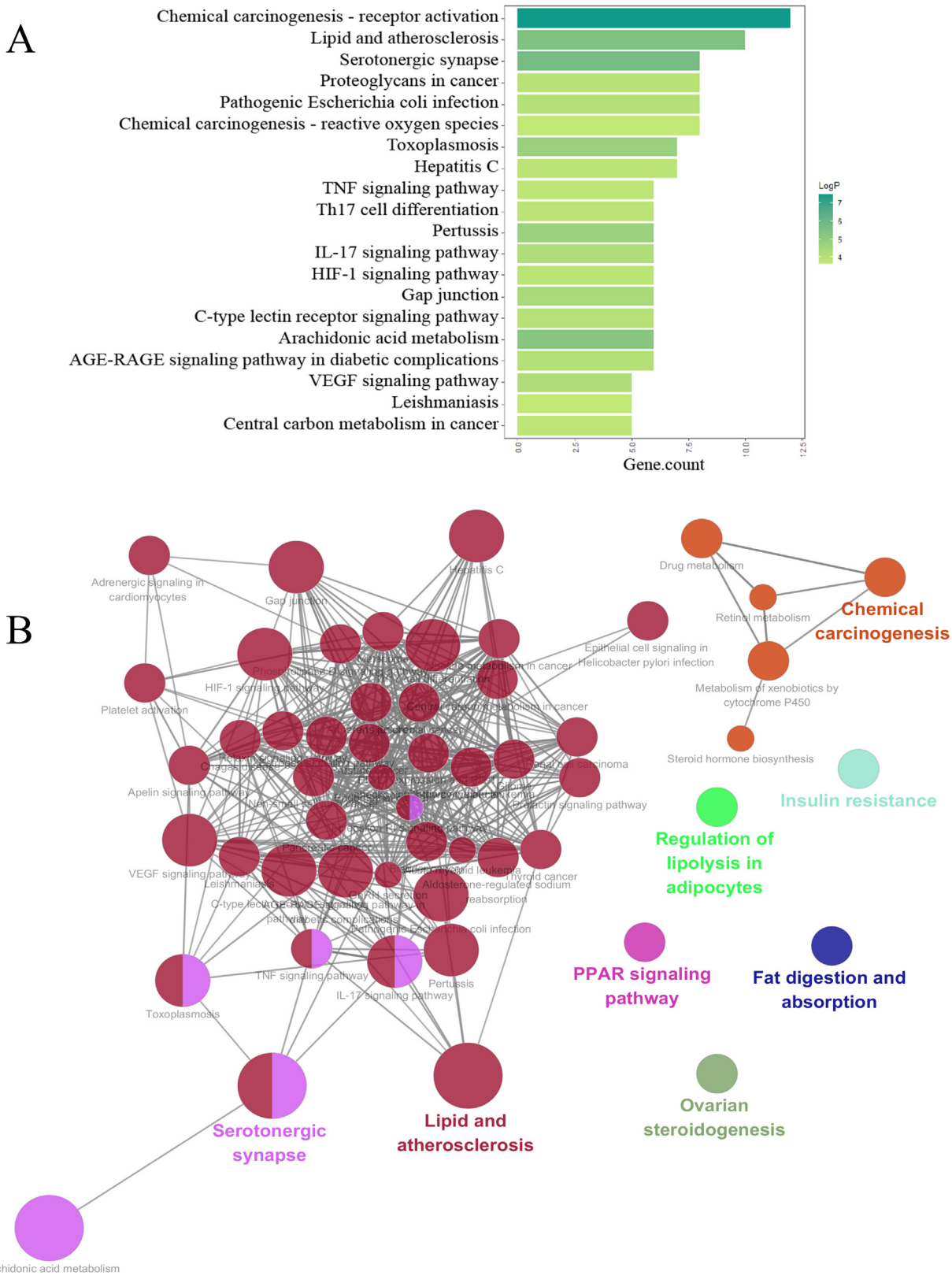

Fig. 10 KEGG pathway enrichment analysis (A) The bar chart on the top 20 significantly enriched KEGG pathway terms by RStudio; (B) The network diagram of KEGG pathway enrichment analysis by clueGO. (Each node indicates the enriched KEGG pathway term, the more significant the *p*-value is, the larger the node is; different colors represent different pathway groups, the bold font is treated as the pathway representation, and the line between nodes means the correlation among pathways).

ID	Description	ID	Description
hsa05207	Chemical carcinogenesis - receptor activation	hsa05130	Pathogenic Escherichia coli infection
hsa04726	Serotonergic synapse	hsa04625	C-type lectin receptor signaling pathway
hsa05417	Lipid and atherosclerosis	hsa05205	Proteoglycans in cancer
hsa00590	Arachidonic acid metabolism	hsa04659	Th17 cell differentiation
hsa05145	Toxoplasmosis	hsa04066	HIF-1 signaling pathway
hsa05133	Pertussis	hsa05160	Hepatitis C
hsa04540	Gap junction	hsa05230	Central carbon metabolism in cancer
hsa04657	IL-17 signaling pathway	hsa04668	TNF signaling pathway
hsa04370	VEGF signaling pathway	hsa05208	Chemical carcinogenesis - reactive oxygen species
hsa04933	AGE-RAGE signaling pathway in diabetic complications	hsa05140	Leishmaniasis

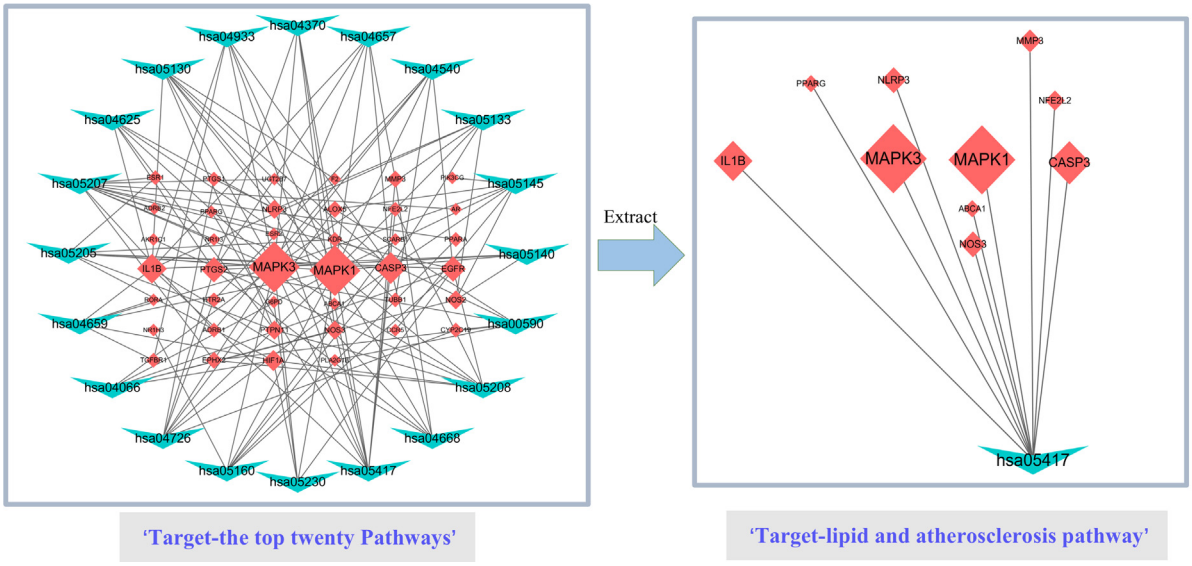

Fig. 11 The network diagram of 'Target-Pathway'.

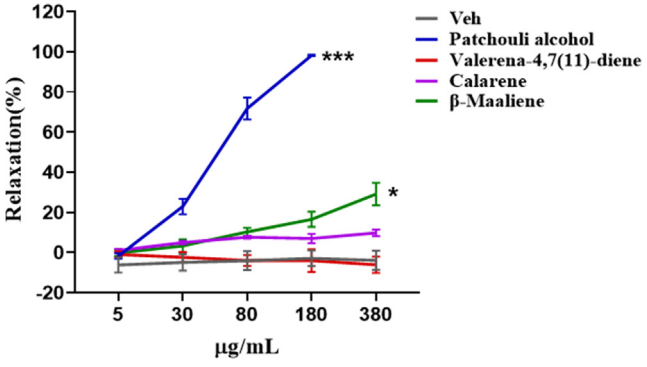

Fig. 12 Dose-vasorelaxant activity graph of β-maaliene, calarene, valerena-4,7(11)-diene and patchouli alcohol (n = 3. *p < 0.05, ***p < 0.001 *vs*. Veh.).

regulators in these pathways and have been identified as upstream regulators. Further, the PPI analysis revealed that all ten selected key targets interact with PI3K and AKT (Fig. S13), indicating that EONJ could potentially treat CVD by modulating the PI3K-AKT signaling pathway. AKT, also known as PKB, plays a crucial role in improving contractile function in the failing heart, and its downregulation is associated with cardiomyocyte damage and apoptosis (Fujio et al., 2000; Shiojima et al., 2012; Wu et al., 2000). Several studies have highlighted the significance of the PI3K-AKT signaling pathway in the treatment of CVD (Fujio et al., 2000; Li et al., 2020; Maiwulanjiang et al., 2014; Shiojima et al., 2012; Wu et al., 2000). EONJ has been shown to prevent oxidative stress-induced cell death by decreasing the production of intracellular ROS in cardiac myocytes, inducing antioxidant enzymes, and activating the phosphorylation of AKT (Maiwulanjiang et al., 2014). Additionally, high doses of EONJ could reduce myocardial infarction after ischemia–reperfusion and lower the levels of CK-MB and cTnT. This study's differential expression of the AKT pathway and phosphorylated proteins suggested that EONJ could protect the heart and reduce myocardial injury by regulating the PI3K-AKT pathway (Yang et al., 2018). Endothelium-derived nitric oxide (NO) is a key vasodilator, while Ang II is one of the endogenous vasoconstrictors. An increase in NO and a decrease in Ang II can induce a vasodilation (Zhang et al., 2019a). The effect of EONJ on vasodilation may also be mediated by the phosphorylation of endothelial nitric oxide synthase (eNOS) via AKT phosphorylation (Maiwulanjiang et al., 2015).

5. Conclusion

This study provides a comprehensive analysis of the vasodilatory activity of the essential oil of *N. jatamansi*, its marker constituents, and the underlying molecular mechanisms. By integrating GC–MS spectrum-

Table 3 Vasodilatory activities of β-maaliene, calarene, valerena-4,7(11)-diene and patchouli alcohol.

Compound	Relaxation (%)					EC_{50} (μg/mL)
	5 μg/mL	30 μg/mL	80 μg/mL	180 μg/mL	380 μg/mL	
Patchouli alcohol	−1.79 ± 1.37	22.91 ± 3.86**	71.71 ± 5.45***	98.20 ± 0.40***	–	51.75
Valerena-4,7(11)-diene	−0.89 ± 1.51	−2.34 ± 2.58	−3.99 ± 2.73	−4.01 ± 5.63	−6.11 ± 4.06	–
Calarene	0.99 ± 0.74	4.91 ± 0.86	7.61 ± 0.71	6.94 ± 2.31	9.77 ± 1.61	–
β-Maaliene	−0.19 ± 1.64	3.32 ± 3.16	10.24 ± 2.01	16.52 ± 3.78*	29.08 ± 5.58*	–

n = 3, *$p < 0.05$ *vs.* Veh, **$p < 0.01$ *vs.* Veh, ***$p < 0.001$ *vs.* Veh.

vasodilatory activity relationship, network pharmacology, and vascular tone tests, we identified two bioactive compounds (patchouli alcohol and β-maaliene) and two critical biological targets (NOS3 and PTGS2) for *N. jatamansi* in the treatment of cardiovascular diseases. Our findings suggest that *N. jatamansi* exerts its vasodilatory effect mainly through lipid and atherosclerosis signaling as well as the PI3K-AKT pathway. This work provides valuable information for the quality evaluation, identification of bioactive markers, and potential industrial applications of *N. jatamansi* for cardiovascular and related disorders.

Declaration of Competing Interest

The authors declare that they have no known competing financial interests or personal relationships that could have appeared to influence the work reported in this paper.

Acknowledgments

The authors would like to express their gratitude to the Tianjin Committee of Science and Technology of China (No. 21ZYJDJC00080 and 22ZYJDSS00040), the National Key Research and Development Program of China (2019YFC1708803), the Innovation Team and Talents Cultivation Program of National Administration of Traditional Chinese Medicine (No: ZYYCXTD-D-202002, ZYYCXTD-C-202203), and the National Key Research and Development Project of China (No. 2018YFC1707905 and 2018YFC1707403) for supporting this research.

Ethical approval

No studies involving human participants were conducted by any of the authors of this article.

Author contributions

The conception and design of the research were performed by H.-H. Wu and Q.-L. Wang. B.-X. Xue and S.-X. Liu conducted the experiments and data analysis collaboratively. B.-X. Xue was responsible for drafting the manuscript with critical input from H.-H. Wu and Q.-L. Wang. P.-K. Oduro contributed to the analysis and visualization of the network pharmacology data. N.-A. M.-Gyimah and L.-H. Zhang assisted with the manuscript revision.

Appendix A. Supplementary material

Supplementary data to this article can be found online at https://doi.org/10.1016/j.arabjc.2023.104911.

References

Abraham, W.-R., Kieslich, K., Stumpf, B., Ernst, L., 1992. Microbial oxidation of tricyclic sesquiterpenoids containing a dimethylcyclopropane ring. Phytochemistry 31 (11), 3749–3755.

Aisa, R., Yu, Z., Zhang, X., Maimaitiyiming, D., Huang, L., Hasim, A., Jiang, T., Duan, M., 2017. The effects of aqueous extract from *Nardostachys chinensis* Batal in on blood pressure and cardiac hypertrophy in two-kidney one-clip hypertensive rats. Evid. Based Complement. Alternat. Med. 2017, 1–11. https://doi.org/10.1155/2017/4031950.

Bhat, M.D.A., Malik, S.A., 2020. Efficacy of *Nardostachys jatamansi* (D.Don) DC in essential hypertension: a randomized controlled study. Complement. Ther. Med. 53, 1–5. https://doi.org/10.1016/j.ctim.2020.102532.

Bose, B., Tripathy, D., Chatterjee, A., Tandon, P., Kumaria, S., 2019. Secondary metabolite profiling, cytotoxicity, anti-inflammatory potential and *in vitro* inhibitory activities of *Nardostachys jatamansi* on key enzymes linked to hyperglycemia, hypertension and cognitive disorders. Phytomedicine 55, 1–45. https://doi.org/10.1016/j.phymed.2018.08.010.

Cai, H., Xu, Y., Xie, L., Duan, Y., Zhou, J., Liu, J., Niu, M., Zhang, Y., Shen, L., Pei, K., Cao, G., 2019. Investigation on spectrum-effect correlation between constituents absorbed into blood and bioactivities of Baizhu Shaoyao San before and after processing on ulcerative colitis rats by UHPLC/Q-TOF-MS/MS coupled with gray correlation analysis. Molecules 24, 1–26. https://doi.org/10.3390/molecules24050940.

Cao, M., Ge, Y.Z., Luo, J., Wang, Y.X., Zhang, S.H., Wu, Z.T., 2010. Effects of volatile oil of *Nardostachys chinensis* on L-type calcium channel in isolated ventricular myocytes in rat. Lishizhen MedMater Med Res. 21, 2264–2266.

Chauhan, R., Nautiyal, M., Kumar, A., 2011. Analysis of variabilities in populations of *Nardostachys jatamansi* DC. in Garhwal Himalaya, India. J. Plant Breeding Crop Sci. 3, 190–194. https://doi.org/10.5897/JPBCS.9000010.

Chauhan, R.S., Nautiyal, M.C., Figueredo, G., Rana, V.S., 2017. Effect of post harvest drying methods on the essential oil composition of *Nardostachys jatamansi* DC. J. Essent. Oil-Bear. Plants. 20, 1090–1096. https://doi.org/10.1080/0972060X.2017.1363001.

Chen, C., Chen, J., Shi, J., Chen, S., Zhao, H., Yan, Y., Jiang, Y., Gu, L., Chen, F., Liu, X., 2019. A strategy for quality evaluation of

salt-treated *Apocyni Veneti* Folium and discovery of efficacy-associated markers by fingerprint-activity relationship modeling. Sci. Rep. 9, 16666. https://doi.org/10.1038/s41598-019-52963-3.

Chen, J., Gai, X., Xu, X., Liu, Y., Ren, T., Liu, S., Ma, T., Tian, C., Liu, C., 2020. Research on quality markers of Guizhi Fuling prescription for endometriosis treatment based on gray correlation analysis strategy. Front. Pharmacol. 11, (1–11). https://doi.org/10.3389/fphar.2020.588549 588549.

Cheng, Q., Chen, X., Wu, H., Du, Y., 2021. Three hematologic/immune system-specific expressed genes are considered as the potential biomarkers for the diagnosis of early rheumatoid arthritis through bioinformatics analysis. J. Transl. Med. 19, 1–15. https://doi.org/10.1186/s12967-020-02689-y.

China Pharmacopoeia Committee, 2020. Pharmacopoeia of the People's Republic of China. Part IV. China Medical Science and Technology Press, Beijing, pp. 233. May 2020.

China Pharmacopoeia Committee, 2020. Pharmacopoeia of the People's Republic of China. Part I. China Medical Science and Technology Press, Beijing, pp. 87–88. May 2020.

Fang, J., Li, R., Zhang, Y., Oduro, P.K., Li, S., Leng, L., Wang, Z., Rao, Y., Niu, L., Wu, H.-H., Wang, Q., 2022. Aristolone in *Nardostachys jatamansi* DC. induces mesenteric vasodilation and ameliorates hypertension via activation of the KATP channel and PDK1-Akt-eNOS pathway. Phytomedicine 104,. https://doi.org/10.1016/j.phymed.2022.154257 154257.

Forstermann, U., Xia, N., Li, H., 2017. Roles of vascular oxidative stress and nitric oxide in the pathogenesis of atherosclerosis. Circ. Res. 120 (4), 713–735. https://doi.org/10.1161/CIRCRESAHA.116.309326.

Fujio, Y., Nguyen, T., Wencker, D., Kitsis, R.N., Walsh, K., 2000. Akt promotes survival of cardiomyocytes *in vitro* and protects against ischemia-reperfusion injury in mouse heart. Circulation 101, 660–667. https://doi.org/10.1161/01.CIR.101.6.660.

Furusawa, M., Hashimoto, T., Noma, Y., Asakawa, Y., 2006. Biotransformation of aristolane- and 2,3-secoaromadendrane-type sesquiterpenoids having a 1,1-dimethylcyclopropane ring by *Chlorella fusca* var. vacuolata, *Mucor Species*, and *Aspergillus niger*. Chem. Pharm. Bull. 54 (6), 861–868.

Geng, X.P., Shi, J.L., Liu, Y., Xiao, P.G., 2011. Comparison of chemical constituents of volatile oil in aerial part and underground part of Gansong (Rhizoma *Nardostachydis*). J Beijing Univ Tradit Chin Med. 34, 56–59.

Guo, L., Gong, M., Wu, S., Qiu, F., Ma, L., 2020. Identification and quantification of the quality markers and anti-migraine active components in *Chuanxiong Rhizoma* and *Cyperi Rhizoma* herbal pair based on chemometric analysis between chemical constituents and pharmacological effects. J. Ethnopharmacol. 246, 1–40. https://doi.org/10.1016/j.jep.2019.112228.Epub 2019 Sep 9.

Han, X., Beaumont, C., Stevens, N., 2017. Chemical composition analysis and *in vitro* biological activities of ten essential oils in human skin cells. Biochim. Open 5, 1–7. https://doi.org/10.1016/j.biopen.2017.04.001.

He, D., Huang, J.H., Zhang, Z.Y., Du, Q., Peng, W.J., Yu, R., Zhang, S.F., Zhang, S.H., Qin, Y.H., 2019. A network pharmacology-based strategy for predicting active ingredients and potential targets of LiuWei DiHuang Pill in treating type 2 diabetes mellitus. Drug Des Dev. Ther. 13, 3989–4005. https://doi.org/10.2147/DDDT.S216644.eCollection 2019.

Hu, G.Y., Peng, C., Xie, X.F., Xiong, L., Zhang, S.Y., Cao, X.Y., 2018. Patchouli alcohol isolated from *Pogostemon cablin* mediates endothelium-independent vasorelaxation by blockade of Ca^{2+} channels in rat isolated thoracic aorta. J. Ethnopharmacol. 220, 188–196. https://doi.org/10.1016/j.jep.2017.09.036.

Huang, C., Dong, M., Luo, J., Qian, H., Zhang, J., Huang, Y., 2020. The activity screening of Hmong herbs *Caesalpiniaminax* and an antitumor effect study. Evid. Based Complement. Alternat. Med. 2020, 1–13. https://doi.org/10.1155/2020/3585736.

Jia, Y., Zou, J., Wang, Y., Zhang, X., Shi, Y., Liang, Y., Guo, D., Yang, M., 2021. Action mechanism of *Roman chamomile* in the treatment of anxiety disorder based on network pharmacology. J. Food Biochem. 45, 1–19. https://doi.org/10.1111/jfbc.13547.

Jiang, C.Y., Ge, Y.Z., Liu, Y.F., Wang, Y.X., Wu, Z.T., Sheng, S.H., 2017. The effects of the volatile oil of Nardostachy chinensis Batal on cardiac sodium currents in salt-sensitive hypertensive rat by injuring sensory nerve. Lishizhen MedMater Med. Res. 28, 2855–2858. https://doi.org/10.3969/j.issn.1008-0805.2017.12.014.

Jin, Q., Xiao, F., Qun, P., Li, Y., Liu, Y., 2018a. Identification of volatile oil components of Nardostachys jatamansi DC. root and rhizome, herb. Med. Plant. 9, 11–15. https://doi.org/10.19600/j.cnki.issn2152-3924.2018.02.004.

Jin, Q., Li, Y., Liu, Z., Qun, P., Liu, Y., 2018b. Comprehensive evaluation of volatile oil of *Nardostachys jatamansi* in different growing areas based on total statistical moment. Chin Tradit. Pat. Med. 40, 2025–2029.

Kong, W.J., Zhang, S.S., Zhao, Y.L., Wu, M.Q., Chen, P., Wu, X.R., Ma, X.P., Guo, W.Y., Yang, M.H., 2017. Combination of chemical fingerprint and bioactivity evaluation to explore the antibacterial components of *Salvia miltiorrhizae*. Sci. Rep. 7, 1–12. https://doi.org/10.1038/s41598-017-08377-0.

Li, L., Yang, D., Li, J., Niu, L., Chen, Y., Zhao, X., Oduro, P.K., Wei, C., Xu, Z., Wang, Q., Li, Y., 2020. Investigation of cardiovascular protective effect of Shenmai injection by network pharmacology and pharmacological evaluation. BMC Complement Med. Ther. 20, 1–15. https://doi.org/10.1186/s12906-020-02905-8.

Liu, X.C., Liu, Z.L., 2014. Evaluation of insecticidal activity of *Nardostachys jatamansi* essential oil against some grain storage insects. J. Entomol. Zool. Stud. 2, 335–340.

Liu, C., Ma, C., Lu, J., Cui, L., Li, M., Huang, T., Han, Y., Li, Y., Liu, Z., Zhang, Y., Kang, W., 2021. A rapid method and mechanism to identify the active compounds in *Malus micromalus Makino* fruit with spectrum-effect relationship, components knock-out and molecular docking technology. Food Chem. Toxicol. 150, 1–14. https://doi.org/10.1016/j.fct.2021.112086.

Lovren, F., Teoh, H., Verma, S., 2015. Obesity and atherosclerosis: mechanistic insights. Can. J. Cardiol. 31, 177–183. https://doi.org/10.1016/j.cjca.2014.11.031.

Lyle, N., Gomes, A., Sur, T., Munshi, S., Paul, S., Chatterjee, S., Bhattacharyya, D., 2009. The role of antioxidant properties of *Nardostachys jatamansi* in alleviation of the symptoms of the chronic fatigue syndrome. Behav. Brain Res. 202, 285–290. https://doi.org/10.1016/j.bbr.2009.04.005.

Maiwulanjiang, M., Chen, J., Xin, G., Gong, A.G., Miernisha, A., Du, C.Y., Lau, K.M., Lee, P.S., Chen, J., Dong, T.T., Aisa, H.A., Tsim, K.W., 2014. The volatile oil of *Nardostachyos* Radix et Rhizoma inhibits the oxidative stress-induced cell injury via reactive oxygen species scavenging and Akt activation in H9C2 cardiomyocyte. J. Ethnopharmacol. 153, 491–498. https://doi.org/10.1016/j.jep.2014.03.010.

Maiwulanjiang, M., Bi, C.W., Lee, P.S., Xin, G., Miernisha, A., Lau, K.M., Xiong, A., Li, N., Dong, T.T., Aisa, H.A., Tsim, K.W., 2015. The volatile oil of *Nardostachyos* Radix et Rhizoma induces endothelial nitric oxide synthase activity in HUVEC cells. PLoS One 10, 1–15. https://doi.org/10.1371/journal.pone.0116761.

Nagashima, F., Tamada, A., Fujll, N., Asakawa, Y., 1997. Terpenoids from the Japanese liver worts Jackiella Javanica and Jungermannia Infusca. Phytochemistry 46 (7), 1203–1208.

Pang, H.Q., Zhou, P., Meng, X.W., Yang, H., Li, Y., Xing, X.D., Wang, H.Y., Yan, F.R., Li, P., Gao, W., 2022. An image-based fingerprint-efficacy screening strategy for uncovering active compounds with interactive effects in Yindan Xinnaotong soft capsule. Phytomedicine 96,. https://doi.org/10.1016/j.phymed.2021.153911 153911.

Parr, J., Lindeboom, W., Khanam, M., Sanders, J., Koehlmoos, T.P., 2012. Informal allopathic provider knowledge and practice regard-

ing hypertension in urban and rural Bangladesh. PLoS One 7 (10), e48056.
Paul, C., Konig, W.A., Muhle, H., 2001. Pacifigorgianes and tamariscene as constituents of *Frullania tamarisci* and *Valeriana officinalis*. Phytochemistry 57, 307–313.
Rehman, T., Ahmad, S., 2019. *Nardostachys chinensis* Batalin: a review of traditional uses, phytochemistry, and pharmacology. Phytother. Res. 33, 2622–2648. https://doi.org/10.1002/ptr.6447.
Saroya, A.S., Singh, J., 2018. Neuropharmacology of *Nardostachys jatamansi* DC, pharmacotherapeutic potential of natural products in neurological disorders. Springer, pp. 167–174.
Shawky, E., El Newehy, N.M., Beltagy, A.M., Abd-Alhaseeb, M.M., Omran, G.A., Harraz, F.M., 2018. Fingerprint profile and efficacy-associated markers of *Nigella sativa* oil for geographical origin determination using targeted and untargeted HPTLC-multivariate analysis. J. Chromatogr. B Anal. Technol. Biomed. Life Sci. 1087–1088, 108–117. https://doi.org/10.1016/j.jchromb.2018.04.042.
Shiojima, I., Schiekofer, S., Schneider, J.G., Belisle, K., Sato, K., Andrassy, M., Galasso, G., Walsh, K., 2012. Short-term akt activation in cardiac muscle cells improves contractile function in failing hearts. Am. J. Pathol. 181, 1969–1976. https://doi.org/10.1016/j.ajpath.2012.08.020.
Takemoto, H., Ito, M., Shiraki, T., Yagura, T., Honda, G., 2008. Sedative effects of vapor inhalation of agarwood oil and spikenard extract and identification of their active components. J. Nat. Med. 62, 41–46. https://doi.org/10.1007/s11418-007-0177-0.
Takemoto, H., Yagura, T., Ito, M., 2009. Evaluation of volatile components from spikenard: valerena-4,7(11)-diene is a highly active sedative compound. J. Nat. Med. 63 (4), 380–385.
Tanaka, K., Komatsu, K., 2008. Comparative study on volatile components of Nardostachys rhizome. J. Nat. Med. 62, 112–116. https://doi.org/10.1007/s11418-007-0199-7.
Wang, F., Liu, S., Luo, M., Qin, Y., Lei, P., Liu, Y., Liang, Y., 2015. Analysis of essential oil of *Nardostachys chinensis* Batal by GC-MS combined with chemometric techniques. Acta Chromatogr. 27, 157–175. https://doi.org/10.1556/AChrom.27.2015.1.12.
Wang, F., Xiong, Z.Y., Li, P., Yang, H., Gao, W., Li, H.J., 2017. From chemical consistency to effective consistency in precise quality discrimination of *Sophora flower-bud* and *Sophora flower*: Discovering efficacy-associated markers by fingerprint-activity relationship modeling. J. Pharm. Biomed. Anal. 132, 7–16. https://doi.org/10.1016/j.jpba.2016.09.042.
Wang, M., Yang, T.T., Rao, Y., Wang, Z.M., Dong, X., Zhang, L.H., Han, L., Zhang, Y., Wang, T., Zhu, Y., Gao, X.M., Li, T.X., Wang, H.Y., Xu, Y.T., Wu, H.H., 2021. A review on traditional uses, phytochemistry, pharmacology, toxicology and the analytical methods of the genus Nardostachys. J. Ethnopharmacol. 280, 1–37. https://doi.org/10.1016/j.jep.2021.114446.
Wang, J., Zhao, J., Liu, H., Zhou, L., Liu, Z., Wang, J., Han, J., Yu, Z., Yang, F., 2010. Chemical analysis and biological activity of the essential oils of two valerianaceous species from China: *Nardostachys chinensis* and *Valeriana officinalis*. Molecules 15, 6411–6422. https://doi.org/10.3390/molecules15096411.
Wu, W., Lee, W.L., Wu, Y.Y., Chen, D., Liu, T.J., Jang, A., Sharma, P.M., Wang, P.H., 2000. Expression of constitutively active phosphatidylinositol 3-kinase inhibits activation of caspase 3 and apoptosis of cardiac muscle cells. J. Biol. Chem. 275, 40113–40119. https://doi.org/10.1074/jbc.M004108200.
Wu, Y., Zhou, J., Min, C.Y., Wu, Y.S., Jin, J.J., Qin, K.M., 2015. Analysis on volatile component of Nardostachys root by using gas chromatography-mass spectroscopy. Tradit. Chin. Med. 8, 550–553. https://doi.org/10.3969/j.issn.1674-1749.2015.05.009.
Xiao, R.Y., Wu, L.J., Hong, X.X., Tao, L., Luo, P., Shen, X.C., 2018. Screening of analgesic and anti-inflammatory active component in Fructus *Alpiniae zerumbet* based on spectrum-effect relationship and GC-MS. Biomed. Chromatogr. 32, 1–26. https://doi.org/10.1002/bmc.4112.
Yang, T., Ge, Y.Z., Luo, J., Hu, L.J., Zhang, S.H., Wu, Z.T., 2010. Effects of volatile oil *Nardostachys chinensis* on sodiun channel in isolated ventricular myocytes in rats. Lishizhen MedMater Med Res. 21, 284–286.
Yang, Z.Y., He, J.H., Lu, A.P., Hou, T.J., Cao, D.S., 2020. Application of negative design to design a more desirable virtual screening library. J. Med. Chem. 63, 4411–4429.
Yang, T., Wang, X.P., Xu, L.G., Ou, Y.F., Xu, T., 2018. Effects of volatile oil of *Nardostachys chinensis* on reperfusion injury and PI3K signaling pathway in myocardial ischemia rats. J Clin. Med. Pract. 22, 14–17.
Yuan, J.-H., Cai, Z.-C., Chen, C.-H., Wu, N., Yin, S.-X., Wang, W.-X., Chen, H.-J., Zhou, Y.-Y., Li, L., Liu, X.-H., 2022. A study for quality evaluation of *Taxilli Herba* from different hosts based on fingerprint-activity relationship modeling and multivariate statistical analysis. Arab. J. Chem. 15, 1–13. https://doi.org/10.1016/j.arabjc.2022.103933.
Zeng, P., Su, H.F., Ye, C.Y., Qiu, S.W., Shi, A., Wang, J.Z., Zhou, X.W., Tian, Q., 2022. A tau pathogenesis-based network pharmacology approach for exploring the protections of *Chuanxiong* rhizoma in Alzheimer's disease. Front. Pharmacol. 13, 1–15. https://doi.org/10.3389/fphar.2022.877806.
Zhang, J., Chen, T., Li, K., Xu, H., Liang, R., Wang, W., Li, H., Shao, A., Yang, B., 2019a. Screening active ingredients of rosemary based on spectrum-effect relationships between UPLC fingerprint and vasorelaxant activity using three chemometrics. J. Chromatogr. B Anal. Technol. Biomed. Life Sci. 1134–1135, 1–27. https://doi.org/10.1016/j.jchromb.2019.121854.
Zhang, Y., Wang, C., Yang, F., Sun, G., 2019b. A strategy for qualitative and quantitative profiling of glycyrrhiza extract and discovery of potential markers by fingerprint-activity relationship modeling. Sci. Rep. 9, 1–11. https://doi.org/10.1038/s41598-019-38601-y.
Zhang, C., Zheng, X., Ni, H., Li, P., Li, H.-J., 2018. Discovery of quality control markers from traditional Chinese medicines by fingerprint-efficacy modeling: Current status and future perspectives. J. Pharm. Biomed. Anal. 159, 296–304. https://doi.org/10.1016/j.jpba.2018.07.006.
Zhao, S., Cheng, C.K., Zhang, C.L., Huang, Y., 2021. Interplay between oxidative stress, cyclooxygenases, and prostanoids in cardiovascular diseases. Antioxid. Redox Signal. 34, 784–799. https://doi.org/10.1089/ars.2020.8105.
Zhou, Y., Zhou, H., Hua, L., Hou, C., Jia, Q., Chen, J., Zhang, S., Wang, Y., He, S., Jia, E., 2021. Verification of ferroptosis and pyroptosis and identification of PTGS2 as the hub gene in human coronary artery atherosclerosis. Free Radic. Biol. Med. 171, 55–68. https://doi.org/10.1016/j.freeradbiomed.2021.05.009.